# Optoelectronic Oscillators (OEOs) to Sensing, Measurement, and Detection

Xihua Zou, *Member, IEEE*, Xinkai Liu, Wangzhe Li, *Member, IEEE*, Peixuan Li, Wei Pan, Lianshan Yan, *Senior Member, IEEE*, and Liyang Shao, *Member, IEEE*

*(Invited Paper)*

***Abstract*— Besides distinct features on RF/optical signal generation, optoelectronic oscillators (OEOs) have also been rapidly developed as emerging techniques towards sensing, measurement, and detection. In this paper, we start with the conceptual architecture and the analytical model of OEOs. Then, three operation principles behind sensing, measurement, and detection applications are categorized, including the variation on the time delay of loop, the passband reconfiguration of microwave photonic filter in loop, and the oscillation gain from injection locking, which clearly clarify the X-to-frequency mapping (X denotes target parameter or signal) for supporting practical solutions and approaches. Next, a comprehensive review to advances in OEO-based sensing, measurement, and detection applications is presented, including length change and distance measurement, refractive index estimation, load and strain sensing, temperature and acoustic sensing, optical clock recovery, and low-power RF signal detection. As a new application example, a novel approach for in-line position finding is proposed. When a long fiber Bragg grating inserted into OEO is locally heated to slightly broaden its reflection spectrum, the target position heated is mapped into the oscillating frequency shift, according to the first operation principle. A sensitivity of 254.66 kHz/cm is obtained for position finding in the experiment. Afterward, solutions for calibration and stabilization are briefly introduced, which enable us to improve the accuracy and reliability. Finally, features and future prospects on the sensing, measurement, and detection applications are discussed, such as compact and integrated OEOs.**

***Index Terms*— Optoelectronic oscillator (OEO), oscillating frequency, sensing and sensor, measurement, detection, position finding, fiber Bragg grating, photonic integrated circuits (PICs).**

Manuscript received September 22, 2015; revised November 2, 2015; accepted November 19, 2015. Date of publication December 3, 2015; date of current version December 31, 2015. This work was supported in part by the National High Technology Research and Development Program of China under Grant 2015AA016903, in part by the International Science and Technology Cooperation Program of China under Grant S2014ZR0271, and in part by the National Natural Science Foundation of China under Grant 61378008. The work of X. Zou was supported by the Research Fellowship of the Alexander von Humboldt Foundation, Germany.

X. Zou is with the Center for Information Photonics and Communications, School of Information Science and Technology, Southwest Jiaotong University, Chengdu 611756, China, and also with the Institute of Optoelectronics, University of Duisburg–Essen, Duisburg 47057, Germany (e-mail: zouxihua@swjtu.edu.cn).

X. Liu, P. Li, W. Pan, L. Yan, and L. Shao are with the Center for Information Photonics and Communications, School of Information Science and Technology, Southwest Jiaotong University, Chengdu 611756, China (e-mail: liuxk20040706@163.com).

W. Li was with the Microwave Photonics Research Laboratory, University of Ottawa, Ottawa, ON K1N 6N5, Canada. He is now with the Departments of Electrical and Computer Engineering and Materials, University of California at Santa Barbara, Santa Barbara, CA 93106 USA.

Color versions of one or more of the figures in this paper are available online at http://ieeexplore.ieee.org.

Digital Object Identifier 10.1109/JQE.2015.2504088

## I. Introduction

OSCILLATIONS are common phenomena and most widely used in our society, inside which periodic energy conversions are implemented or sustained. Such oscillations refer to for instance traditional mechanical oscillators (e.g., clock pendulum, spring-mass system), electromagnetic ones, atomic or quantum mechanical ones [1]–[7].

Among these oscillators, the electromagnetic ones are essential to electrical engineering, information technology, and computer science. Such oscillators originate from the oscillating arch built by E. Thomson in 1892 [8], followed by the invented vacuum tube oscillators using feedback or "regeneration" in 1912 [9]. Nowadays, we can find a wide variety of notable electromagnetic oscillators, such as piezoelectric quartz resonator, maser, laser, and optoelectronic oscillator (OEO).

The objective of this paper is OEO, of which the concept dates back to the paper of R. T. Kersten in 1978 [10]. Then, some prototypes to OEOs were designed using directly modulated laser sources or free space optics [11]–[18]. Next, X. S. Yao and L. Maleki developed OEOs by using fiber-optic devices and achieved excellent specification in phase noise for the generated microwave signal [19]–[21].

Inside the OEO, a hybrid oscillating loop consisting of both optical and electronic elements and links, is capable of forming self-sustained oscillation to generate both radio-frequency (RF) and optical signals based on the hybrid gain or feedback from the electrical and the optical domains. More importantly, the energy-storage capability can be significantly improved to offer extremely high spectral purity, by using long optical link with low loss and low dispersion in RF bands or high-Q optical resonators [e.g., whispering-gallery-mode resonators (WGMR) or Kerr frequency comb [22]]. These features are usually very complex or even not directly possible to be achieved by using pure electronic techniques. Meanwhile, large bandwidth and frequency-independent loss of optical components and links are greatly beneficial for us to achieve unprecedented frequency agility.

Consequently, as one of key optoelectronic units [23], OEOs have already been implemented in numerous applications in terms of the generation, distribution, processing, and detection of electromagnetic signals. In particular, OEOs are inevitable for almost any system that transmits or/and receives electromagnetic signals, and extensively used in communications, radar, signal processing, sensor, metrology, radio astronomy [24]. In the following, quintessential applications

are listed, including signal generation, sensing, measurement, and detection.

### A. Generation of Continuous-Wave RF Signals

As demonstrated above, to OEO the most concerned is its capability of generating continuous-wave (CW) RF signals with ultra-low phase noise. From the first OEO prototype released in 1994, a 9.2-GHz oscillating signal with a linewidth of 100 Hz was generated [19]. Stemming from this prototype, a series of specific theories, devices, architectures, and solutions have been proposed to facilitate the implementation of OEOs. Directly modulated lasers were used to reduce power consumption [25], and dual-loop or multi-loop architectures were used to suppress the sideband spurious and to reduce the phase noise simultaneously [26]–[33], including polarization diversity, wavelength diversity, or cascaded rings. Also, the frequency stability and the spectral purity of OEOs can be optimized through injection locking, intra-loop Fabry-Perot etalons, or high-Q filters [34]–[40]. For instance, the spectral purity in coupled OEOs can be greatly enhanced to enjoy an extremely low phase noise, approaching $-160$ dBc/Hz at 10-kHz offset as predicted [39].

In terms of frequency coverage and frequency agility, frequency-doubled or frequency-multiplied OEOs have been implemented using biased Mach–Zehnder modulator (MZM), polarization modulator (PolM) in conjunction with polarizers, or signal processing based on stimulated Brillouin scattering (SBS) effect [41]–[48]. Thus, high-frequency microwave/millimeter-wave signals can be generated from OEOs using low-frequency electronic elements, with the limit on high-frequency narrow electrical filters and amplifiers relieved. Also, tunable microwave photonic filters (MPFs) enrich OEOs in wide and continuous frequency agility [49]–[54]. Such MPFs can be realized through multi-tap architecture, spectrally sliced broadband light source, and phase modulation to intensity modulation (PM-IM) conversion by using dispersive elements, chirped fiber gratings, phase-shifted fiber Bragg grating (PS-FBG), or asymmetric filtering. In [51], for example, a microwave signal with frequency tuned from 3 to 28 GHz was demonstrated by optically adjusting the wavelength difference between the optical carrier and the notch of PS-FBG.

### B. Generation of Pulsed Signals and Complex Waveforms

Besides CW tones, pulsed signals and complex waveforms can be generated using OEOs, both in the RF domain and in the optical domain.

According to the nonlinear dynamics or the dynamic instabilities [55]–[59], broadband chaotic RF signals were produced at the output of OEOs, such as chaos with a flat power spectral density of 8 GHz [57] and a chaotic ultra-wideband (UWB) signal [59].

When RF tones originating from OEO loops are selected as the seed, the generation of phase-coded, linearly-chirped, triangular, and even arbitrary RF waveforms is greatly facilitated, as being assisted by additional modulators or filters [60]–[62]. Such complex waveforms can find significant applications in advanced communications, radar, and electronic warfare.

In addition to RF signals, optical pulses with low time jitter and high repetition rate are valuable products from OEOs [63]–[71], owing to the unique feature providing both electrical and optical outputs simultaneously. Moreover, there are available optical frequency combs implemented using OEOs [72]–[74].

### C. OEOs to Sensing, Measurement, and Detection

In recent years, emerging applications of OEOs to sensing, measurement, and detection have intensively developed and attracted much attention. Among these applications, in general, the target parameter or signal (say X) to be measured is converted to the frequency shift of oscillating signals of OEOs, and we define this procedure as an X-to-frequency mapping or coding. Then an analysis of the oscillating frequency in the electrical domain tells the target parameter or signal. Therefore, high resolution and high signal-to-noise ratio (SNR) can be ensured.

Regarding the details of OEO-based sensing, measurement, and detection, a considerable number of approaches have already been demonstrated to measure target parameters or signals, including such as distance, length change, refractive index, temperature, transverse load, strain, and RF/optical signals. Thus, there will be huge space and great prospects for such applications using OEOs, and we will focus on this topic.

The remainder of this paper is organized as follows. In Section II, the conceptual architecture and the analytical model to OEOs will be introduced. In Section III, three categories of operation principles behind the sensing, measurement, and detection using OEOs are summarized, i.e., the variation on the time delay of loop, the passband reconfiguration of MPF in loop, and the oscillation gain from injection locking, respectively. Section IV is devoted to review diverse applications of sensing, measurement, and detection in recent years, ranging from length change and distance measurement, temperature acquisition, refractive index detection, acoustic sensing, load or train sensing, to low-power RF signal detection and optical clock recovery. Next, as a new application, a novel OEO-based approach for position finding is firstly proposed and experimentally demonstrated with details in Section V. After the overall review and the detailed demonstrations, Section VI describes calibration and stabilization solutions for OEOs. As for future trends and prospects in Section VII, compact and integrated OEOs towards sensing, measurement, and detection are anticipated and preferred. Finally, conclusion will be given in Section VIII.

## II. Conceptual Architecture and Analytical Model

As for the applications to sensing, measurement, and detection, we start with the conceptual architecture and the analytical model of OEOs.

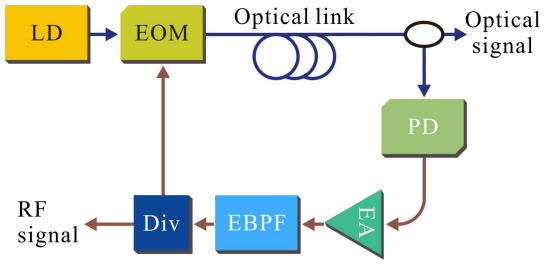


Fig. 1. Schematic diagram of OEO. LD, laser diode; EOM, electro-optic modulator; PD, photodetector; EA, electrical amplifier; EBPF, electrical bandpass filter; Div, divider.

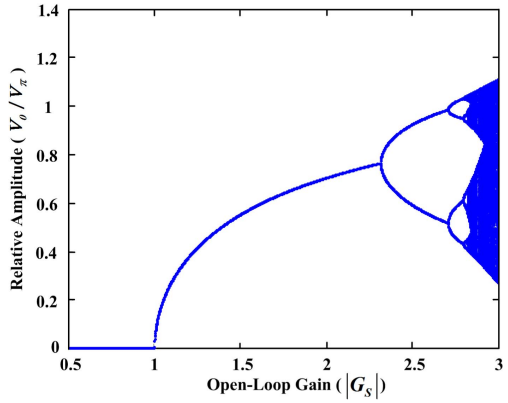


Fig. 2. Distribution of the relative amplitude versus the open-loop gain.

### A. Conceptual Architecture

A generic OEO architecture is shown in Fig. 1, the key part of which is a positive feedback loop consisting of a laser diode (LD), an electro-optic modulator (EOM), a photodetector (PD), an electrical amplifier (EA), and an electrical bandpass filter (EBPF). Firstly, the optical signal from the LD is modulated by an RF signal in the EOM, and sent to a long optical link to introduce a large time delay. A PD is then employed to convert the optical signal to an RF one which is fed back to the EOM after frequency selection and signal amplification. Starting from transient noise, a stable oscillation will be established to provide both low-phase-noise RF signals and low-time-jitter optical pulses, once the power of the input signal to the EOM is equal to the power of the output signal of the EBPF.

### B. OEO Model

Analytical models for OEOs can be found in Refs. [14], [16] released in the 1980s. In this paper, we employ the one established in 1996 based on the quasi-linear theory [20]. In conjunction with Fig. 1, the oscillation process of OEO can be described mathematically step by step as follows. Firstly, a transmission equation of the optical link is defined to bridge the output of the EA with the input of the EOM, as

$$V_{out}(t) = V_{ph}\{1 - \eta \sin \pi [V_{in}(t)/V_\pi + V_B/V_\pi]\}, \quad (1)$$

where $\eta$ determines the extinction ratio of the EOM by $(1+\eta)/(1-\eta)$, $V_B$ and $V_\pi$ are the bias voltage and the half-wave voltage of the EOM. $V_{ph} = (\alpha P_0 \rho/2) RG_A$ is the photovoltage, where $\alpha$ is the fractional insertion loss of the EOM, $P_0$ is the input optical power, $\rho$ and $R$ are the responsivity and the load impedance of the PD, and $G_A$ is the amplifier's voltage gain.

From (1), the link gain (i.e., the open-loop gain, $G_S$) of the OEO can be calculated as

$$G_S = \left.\frac{dV_{out}}{dV_{in}}\right|_{V_{in}=0} = -\frac{\eta\pi V_{ph}}{V_\pi}\cos\left(\frac{\pi V_B}{V_\pi}\right). \quad (2)$$

Assume a sinusoidal wave is applied to the EOM, i.e., $V_{in}(t) = V_0 \sin(\omega t + \beta)$, where $V_0$, $\omega$ and $\beta$ are the amplitude, the angular frequency, and the initial phase of the sinusoidal signal. Then, (1) can be expanded as

$$\begin{aligned} V_{out}(t) = V_{ph}\Bigg\{1 - \eta\sin\left(\frac{\pi V_B}{V_\pi}\right)\Bigg\{J_0\left(\frac{\pi V_0}{V_\pi}\right) \\ +2\sum_{m=1}^{\infty} J_{2m}\left(\frac{\pi V_0}{V_\pi}\right)\cos[2m(\omega t+\beta)]\Bigg\} \\ -2\eta\cos\left(\frac{\pi V_B}{V_\pi}\right)\sum_{m=0}^{\infty} J_{2m+1}\left(\frac{\pi V_0}{V_\pi}\right)\sin \\ \times[(2m+1)(\omega t+\beta)]\Bigg\}, \end{aligned} \quad (3)$$

where $J_m(\cdot)$ denotes the $m$-th order Bessel function of the first kind. When an ideal EBPF is used to refine $V_{out}$, the output of the EBPF (i.e., $V'_{out}$) can be written in terms of the input of the EOM as

$$V'_{out}(\mathrm{t}) = G_\mathrm{s}\frac{2V_\pi}{\pi V_0}J_1\left(\frac{\pi V_0}{V_\pi}\right)V_{in}(t). \quad (4)$$

Based on (4), the operation process of the OEO can be described by the following iterative equations:

$$\tilde{V}_i(\omega,t) = \tilde{F}(\omega)\,G(V_{i-1})\,\tilde{V}_{i-1}(\omega, t-\tau'), \quad (5a)$$

$$G(V_i) = G_\mathrm{s}\frac{2V_\pi}{\pi V_{i-1}}J_1\left(\frac{\pi V_{i-1}}{V_\pi}\right), \quad (5b)$$

$$\tilde{V}_{i=0}(\omega,t) = \tilde{V}_\mathrm{in}(\omega,t), \quad (5c)$$

where $i$ is the order of cycle, $\tilde{V}_i(\omega,t)$, $G(V_i)$, $V_i$ are the oscillating signal between the EBPF and the EOM, the loop gain coefficient, and the oscillating amplitude of the $i$-th cycle, and $\tilde{V}_\mathrm{in}(\omega,t)$ is the transient noise. $\tilde{F}(\omega) = F(\omega)\exp[i\phi(\omega)]$ is a combined effect of all frequency-dependent components in the loop, where $F(\omega)$ and $\phi(\omega)$ are the amplitude and the phase induced by this combined effect. Here, $\tau'$ is the total delay arising from the physical length of the OEO loop [20].

From (5), the distribution of the oscillating amplitude can be revealed, as shown in Fig. 2. When the open-loop gain is larger than 1 but less than 2.31, a constant oscillating amplitude can be obtained to keep a stable oscillation. Beyond the threshold of 2.31, however, periodic or chaotic behaviors occur, leading to the generation of periodic or chaotic signals [56], [75].

When a stable oscillation occurs, the closed-loop gain is actually less than 1. Therefore, a sum of (5a) yields the output

RF power of the OEO, as

$$P(\omega) = \frac{G_A^2 \left|\tilde{V}_{in}(\omega, t)\right|^2 / (2R)}{1 + \left|\tilde{F}(\omega) G(V_0)\right|^2 - 2\left|\tilde{F}(\omega) G(V_0)\right| \cos\left[\omega\tau' + \phi(\omega) + \phi_0\right]}, \tag{6}$$

where $\phi_0$ is the phase factor related to the bias of the EOM.

In case of a free-running OEO without EBPF, a number of periodic oscillating peaks will survive, and the corresponding oscillating frequencies are determined by

$$\omega\tau' + \phi(\omega) + \phi_0 = 2k\pi, \quad k = 0, 1, 2, \ldots\ldots. \tag{7}$$

Therefore, the free spectral range (i.e., FSR, or mode spacing) and the oscillating frequency are obtained as

$$FSR = \frac{1}{\tau} = \frac{1}{\tau' + d\phi(\omega)/d\omega}, \tag{8}$$

$$f_{osc} = (k - \phi_0/2\pi) \times FSR. \tag{9}$$

Here $\tau$ is the total delay of the OEO loop, which is defined as the sum of delays induced by the physical length and the dispersion [20]. In accordance with (8) and (9), sensing, measurement, and detection applications are realized by analyzing the oscillating frequency or/and the FSR, when one, two, or multiple oscillating modes are selected with/without EBPF.

## III. Three Operation Principles to Sensing, Measurement, and Detection

As demonstrated in Section II, the information carried by the oscillating frequency or/and the FSR can be used for the purpose of sensing, measurement, and detection. On the other hand, for detailed approaches and practical solutions, we have to establish a relationship between the oscillating frequency (or/and the FSR) and the target parameter or signal, the defined X-to-frequency mapping or coding aforementioned in Section I. In this section, three key categories of operation principles are summarized and presented to clarify the desired relationship.

### A. Variation on Time Delay of Loop

When the time delay of OEO is varied by a small value of $\Delta\tau$, the perturbations into the FSR and the oscillating frequency are calculated as

$$\Delta FSR = \frac{1}{\tau} - \frac{1}{\tau + \Delta\tau}, \tag{10}$$

$$\Delta f_{osc} = k\left(\frac{1}{\tau} - \frac{1}{\tau + \Delta\tau}\right). \tag{11}$$

This time delay variation actually reflects the change into the loop length, $c\Delta\tau = n\Delta L + L\Delta n$, where $n$ and $\Delta n$ are the effective refractive index and its change, $c$ is the light velocity in vacuum, and $L$ and $\Delta L$ is the physical length and its change. Therefore, any impact contributing to the physical length and the effective refractive index can be measured, including length change, distance, position, temperature, refractive index, strain, vibration, and so on.

### B. Passband Reconfiguration of MPF in Loop

Recently, high Q-factor optical filter is introduced into OEO for implementing MPF, to select oscillating frequency within large bandwidth. Such optical filters include PS-FBG, micro-ring resonator, WGMR, Fabry-Perot cavity, etc. Generally, the central frequency of the MPF (i.e., $f_{MPF}$) is determined by the frequency difference between the LD and the peak/notch of the optical filter:

$$f_{MPF} = |\nu_{LD} - \nu_m|, \quad m = 1, 2, 3\ldots\ldots, \tag{12}$$

where $\nu_{LD}$ and $\nu_m$ are the frequencies of the LD and of the $m$-th peak/notch of the optical filter, respectively. Under the condition of single-mode oscillation, the oscillating frequency of the OEO is approximately equal to the central frequency of MPF, namely $f_{osc} \approx f_{MPF}$. Consequently, a change in the frequency difference will yield an oscillating frequency shift, described as

$$\Delta f_{osc} \approx |\Delta\nu_{LD} - \Delta\nu_m|, \quad m = 1, 2, 3\ldots\ldots. \tag{13}$$

where $\Delta\nu_{LD}$ and $\Delta\nu_m$ are the frequency changes to the LD and to the $m$-th peak/notch of the optical filter, respectively. As a result, any impact contributing to $\Delta\nu_{LD}$ or $\Delta\nu_m$ can be estimated from the oscillating frequency shift, such as transverse load, temperature, and frequency tuning of LD.

### C. Oscillation Gain From Injection Locking

When an injection signal is sent into an OEO through optical or electrical injection, the hybrid signals nearby might get more power/gain from oscillation than others, due to gain competition. In this case, the originally located oscillating modes will be suppressed and a new oscillating mode will be locked to the frequency range of the injection signal, providing the so-called oscillation gain to the injection signal.

As the injection signal is described by $p(t) = p_0(1 + z\sin\omega t)$ [76], the output of the EA can be written as

$$V_{out}(t) = \frac{V_{ph}\, p(t)}{p_0}\left\{1 - \eta\sin\pi\left[V_{in}(t)/V_\pi + V_B/V_\pi\right]\right\}, \tag{14}$$

where $z$ is the modulation index, $p_0$ is the amplitude of the injection signal, and $\omega$ is the angular frequency of the injection signal. While a single mode is remained, it can be expressed as

$$V'_{out}(t) = V_{ph}\left[A\sin(\omega t) + B\cos(\omega t)\right], \tag{15}$$

where

$$A = -2\eta\cos\left(\frac{\pi V_B}{V_\pi}\right) J_1\left(\frac{\pi V_0}{V_\pi}\right)\cos\beta + z\left\{1 - \eta\sin\left(\frac{\pi V_B}{V_\pi}\right)\left[J_0\left(\frac{\pi V_0}{V_\pi}\right) - J_2\left(\frac{\pi V_0}{V_\pi}\right)\cos 2\beta\right]\right\} \tag{16a}$$

$$\mathrm{B} = -2\eta\cos\left(\frac{\pi V_B}{V_\pi}\right) J_1\left(\frac{\pi V_0}{V_\pi}\right)\sin\beta - z\eta\sin\left(\frac{\pi V_B}{V_\pi}\right) J_2\left(\frac{\pi V_0}{V_\pi}\right)\sin 2\beta. \tag{16b}$$

Therefore, the output of the EBPF can be described as

$$V'_{out}(t) = V_{ph}\sqrt{A^2 + B^2}\sin\left[\omega(t-\tau) + \beta_1\right], \quad (17)$$

where $\beta_1 = \arctan(B/A)$. Under a stable oscillation, from (17) we should have

$$V_{ph}\sqrt{A^2 + B^2} = V_0, \quad (18)$$

$$\omega(t-\tau) + \beta_1 = \omega t + \beta - 2k\pi. \quad (19)$$

Also, the angular frequency of the injection signal can be written as

$$\omega = 2\pi\left(f_{osc} \pm \Delta f_B/2\right), \quad (20)$$

where $\Delta f_B$ is the frequency offset of the injection signal with respect to the oscillating frequency. In most cases, $\Delta f_B$ is defined as the locking range or the gain bandwidth, which indicates that only the injection signal falling within this bandwidth can be effectively amplified. By combing (19) and (20), as the maximum negative and positive frequency offsets are considered as an entire band, the locking range of the OEO is derived as

$$\Delta f_B = \frac{\beta_1 - \beta}{2\pi\tau}. \quad (21)$$

Usually, the injection locking is used to reduce the phase noise and to improve the stability of the OEO. Here we have to highlight that the injection locking can also provide oscillation gain to injection signals within the locking range, which is just the principle behind OEO-based optical clock recovery and lower-power RF signal detection.

## IV. Overall Review to Diverse Applications

Assisted by the analytical model and the operation principles above, diverse applications to sensing, measurement, and detection have already been realized using OEOs. In this section, an overall review on these advances will be presented, including length change and distance measurement, refractive index estimation, load and strain sensing, temperature and acoustic sensing, signal detection or recovery, and others.

### *A. Length Change and Distance Measurement*

Length change and distance measurement is one of essential functions in academic community, industry, and daily life. By using oscillation or resonance effect, fine resolution can be offered for distance or length measurement, especially when high-order mode is selected according to the accumulative magnification theory.

As a hybrid oscillator, OEOs show distinct performances in distance or length change measurement [77]–[79]. OEOs are capable of generating RF oscillating signals from fundamental mode to high-order mode with high frequency, narrow linewidth, and low phase noise, such that an analysis on the oscillating frequency leads to a fine resolution and a high SNR for measurements.

In [78], we proposed such approaches for optical length change measurement, as shown in Fig. 3. Here, the use of an amplified spontaneous emission (ASE) source and no EBPF help us reduce the complexity for stabilization control and

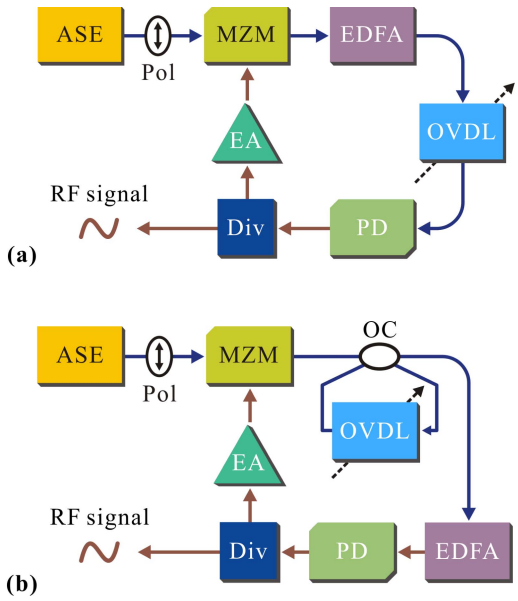


Fig. 3. OEO-based approaches for length change measurement. ASE, amplified spontaneous emission; Pol, polarizer; MZM, Mach–Zehnder modulator; OC, optical coupler; OVDL, optical variable delay line; EDFA, Erbium doped fiber amplifier; PD, photodetector; Div, divider; EA, electrical amplifier; RF, radio frequency.

the cost, while the performance is comparable to that using laser source. For the OEO structure shown in Fig. 3(a), the relationship between the optical length change and the oscillating frequency shift can be derived from (11), which is

$$\Delta f_{osc} \approx -\frac{kc}{nL^2}\Delta L, \quad (22)$$

where $L$ is the total length of the OEO loop and $\Delta L$ is the optical length change. Then, an additional recirculating delay line (RDL) acting as an optical filter is introduced to enlarge the FSR of the OEO, as shown in Fig. 3(b). Besides (22), another linear relationship is added to jointly determine the oscillating frequency shift, as

$$\Delta f_{osc} \propto -\frac{k_1 c}{nL_1^2}\Delta L_1, \quad (23)$$

where $L_1$, $\Delta L_1$, and $k_1$ are the total length, the optical length change, and the order of oscillating mode of the RDL, respectively.

From (22) and (23), a linear relationship between the optical length change and the oscillating frequency shift is established, thus the optical length change can be measured by monitoring the frequency shift of the oscillating signals and the sensitivity can be flexibly improved by choosing a higher-order oscillating mode. Some experimental results are illustrated in Fig. 4. When the fundamental mode (i.e., $k = 1$) is selected, a sensitivity of $-28$ kHz/cm is obtained within the range of 0-10 cm. Moreover, for a high-order mode (i.e., $k = 17$), a higher sensitivity of $-480$ kHz/cm is achieved, which can be further improved by flexibly choosing a much higher-order mode.

While in [79], a dual-loop OEO was proposed to perform the high-precision distance measurement. As shown in Fig. 5, two wavelengths are used to construct two loops, one defined as the measurement oscillator and the other as the reference

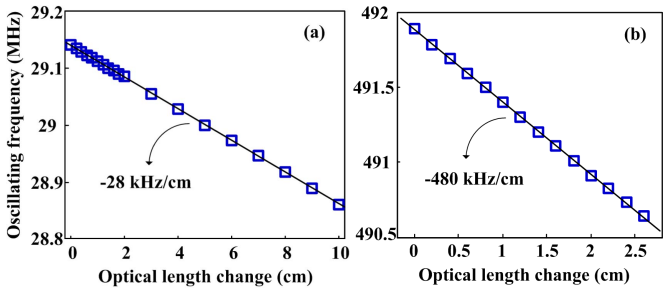


Fig. 4. Measurement sensitivities to the optical length change by selecting (a) fundamental mode (k=1) and (b) high-order mode ( k=17).

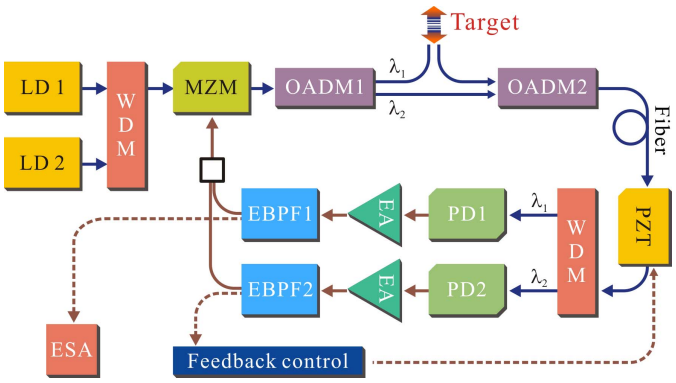


Fig. 5. OEO-based approach for distance measurement. LD, laser diode; WDM, wavelength-division multiplexer; MZM, Mach–Zehnder modulator; OADM, optical add–drop multiplexer; PZT, piezoelectric ceramic transducer; PD, photodetector; EA, electrical amplifier; EBPF, electrical bandpass filter; ESA, electrical signal analyzer.

oscillator. The measurement principle is identical to that mentioned in (22). Here, a feedback setup performed by using a phase-locked loop (PLL) and a piezoelectric ceramic transducer is used to control the loop length, resulting in a reduction of the environmental interferences and an improvement to the accuracy.

In the experiment, the measurement oscillator operated at 20 GHz for high sensitivity, while the reference oscillator at 5 GHz for easy feedback control. The resulting measurement errors were less than $\pm 1.5$ $\mu$m and the maximum uncertainty was less than 3.5 $\mu$m.

### B. Refractive Index Estimation

OEOs also show excellent features in property analysis of materials and compounds, such as refractometer or refractive index estimation [80], [81].

Figure 6 shows the block diagram of such an OEO-based system, where a glass cell is inserted into the OEO loop [80]. By comparing the oscillating frequencies obtained as the cell is filled with and without a target material, the refractive index (i.e., $n_x$) of the material can be derived as

$$n_x = n_{air} + \left| \frac{kc}{f_{osc}^2 l} \Delta f_{osc} \right|, \tag{24}$$

where $n_{air}$ is the refractive index of the air, and $l$ is the inner size of the glass cell.

In the experiment, four liquid materials (i.e., Acetone, Acetonitrile, Dioxane, and Dioxolane) were tested for

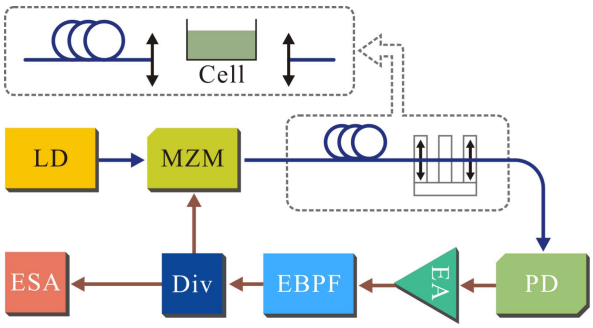


Fig. 6. Refractive index estimation using OEO. LD, laser diode; MZM, Mach–Zehnder modulator; PD, photodetector; EA, electrical amplifier; EBPF, electrical bandpass filter; Div, divider; ESA, electrical signal analyzer.

refractive index estimation. The maximum standard deviation of the measurement results was 0.0031 by using a 500-m fiber loop and a 10-mm quartz cell [81].

### C. Load and Strain Sensing

At the mean time, OEOs provide enabling solutions for applications such as load or strain sensing [82]–[84].

In [83], a transverse load sensor was implemented using a dual-mode OEO. As shown in Fig. 7, a PolM in combination with a PS-FBG is employed to perform mode selection, instead of an EBPF. Due to the birefringence, the PS-FBG has two notches at different wavelengths corresponding to two orthogonal polarization states, as depicted in Fig. 7(b). The two notches are used to perform PM-IM conversion, and two bandpass MPFs with different central frequencies will be resulted, as shown in Fig. 7(c). Thanks to the two MPFs implemented synchronously, this OEO simultaneously has two oscillating frequencies which are described as

$$f_{osc-x} = \nu_{LD} - \nu_x, \tag{25a}$$

$$f_{osc-y} = \nu_{LD} - \nu_y, \tag{25b}$$

where $\nu_{LD}$ is the frequency of the optical carrier, $\nu_x$, $\nu_y$ are the central frequencies of two notches along the two orthogonal polarization states. A beating signal then is generated from the two oscillating signals and its frequency is written as

$$f_{beat} = \left| f_{osc-x} - f_{osc-y} \right| = \left| \nu_x - \nu_y \right| = |cb/(n_0 \lambda_0)|, \tag{26}$$

$$b = 2n_0^3 \left( p_{11} - p_{12} \right) \left( 1 + \nu_p \right) \cos\left( 2\theta \right) F/(\pi r \varepsilon), \tag{27}$$

where $b$ is the load-induced birefringence, $n_0$ is the averaging refractive index of the fiber, $\lambda_0$ is the Bragg wavelength, $p_{11}$ and $p_{12}$ are the components of the strain optical tensor of the optical material, $\nu_p$ is the Poisson ratio, $\varepsilon$ is the Young's modulus, $r$ is the radius of the fiber, $\theta$ is the angle between the direction of the force and the polarization axis of the fiber, and $F$ is the transverse load.

From (26) and (27), the transverse load can be monitored by measuring the beating frequency. The experimental results are indicative of a sensitivity of 9.73 GHz/(N/mm) which agrees with the theoretical value of 9.6 GHz/(N/mm) [83].

Next, Ref. [84] provided an improved solution using an injection-coupled OEO for load sensing. As shown in Fig. 8,

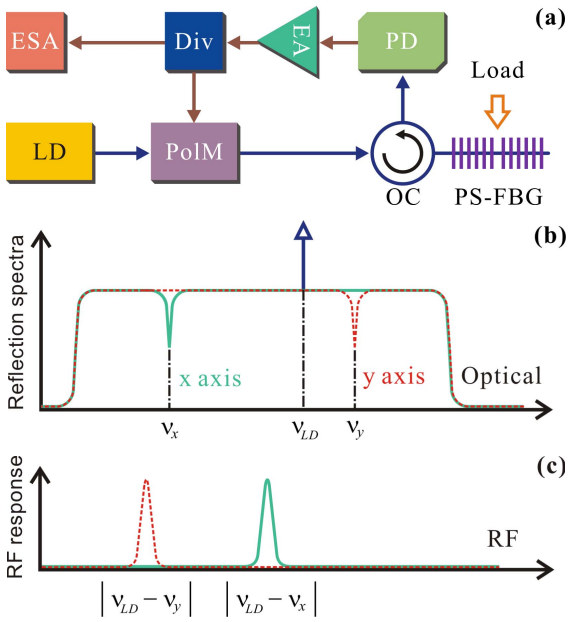


Fig. 7. OEO-based approach for transverse load sensing: (a) schematic diagram; (b) reflection spectra of the PS-FBG along the two orthogonal polarization states; (c) frequency responses of two MPFs. LD, laser diode; PolM, polarization modulator; PS-FBG, phase-shifted fiber Bragg grating; PD, photodetector; EA, electrical amplifier; Div: divider; ESA, electrical signal analyzer.

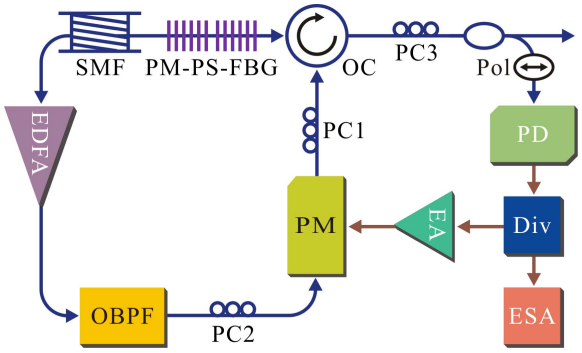


Fig. 8. Improved OEO-based approach for transverse load sensing. EDFA, Erbium doped fiber amplifier; OBPF, optical bandpass filter; PC, polarization controller; PM, phase modulator; PM-PS-FBG, polarization-maintaining phase-shifted fiber Bragg grating; SMF, single mode fiber; Pol, polarizer; PD, photodetector; Div, divider; EA, electrical amplifier; ESA, electrical signal analyzer.

the setup consists of a fiber ring laser and an OEO loop. The fiber ring laser operates at two different wavelengths (i.e., $\lambda_1$ and $\lambda_2$) corresponding to the two notches of polarization-maintaining PS-FBG (PM-PS-FBG) along the two orthogonal polarization states. When the wavelength at $\lambda_1 = c/\nu_x$ is injected into OEO loop as an optical source, an oscillating signal with its frequency expressed as (28) is generated. Likewise, the same thing happens to the other wavelength at $\lambda_2 = c/\nu_y$. In this way, a mutual injection locking is formed between the two oscillations at the two wavelengths, leading to a more stable oscillating frequency.

$$f_{osc} = |\nu_x - \nu_y| = \left|2cn_0^2\left(p_{11}-p_{12}\right)\left(1+\nu_p\right)\cos\left(2\theta\right)F/(\lambda_0\pi r\varepsilon)\right|. \tag{28}$$

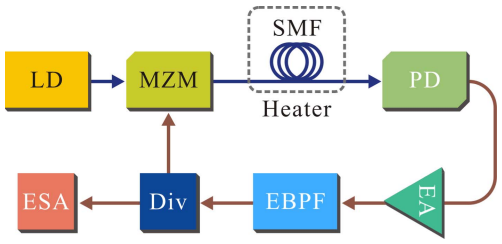


Fig. 9. OEO-based approach for temperature sensing. LD, laser diode; MZM, Mach–Zehnder modulator; SMF, single mode fiber; PD, photodetector; EA, electrical amplifier; EBPF, electrical bandpass filter; Div, divider; ESA, electrical signal analyzer.

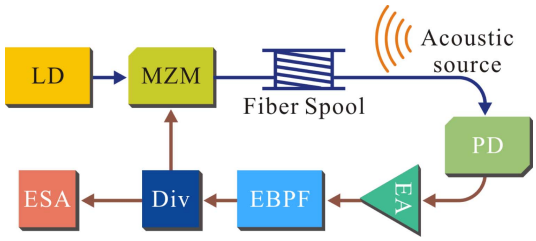


Fig. 10. Acoustic sensing using OEO. LD, laser diode; MZM, Mach–Zehnder modulator; PD, photodetector; EA, electrical amplifier; EBPF, electrical bandpass filter; Div, divider; ESA, electrical signal analyzer.

Therefore, the transverse load can be calculated from the oscillating frequency by following (28). The sensitivity of the sensor was experimentally measured as +9.754 and −9.735 GHz/(N/mm) [84], when the transverse load was applied along the fast and slow axes, respectively.

### *D. Temperature and Acoustic Sensing*

OEOs can also be used to implement temperature and acoustic sensing.

Such a temperature sensor was proposed and experimentally demonstrated in Ref. [85], as shown in Fig. 9. When the single mode fiber (SMF) is heated, the total delay of the OEO loop changes due to the physical length change (i.e., $\Delta L$) and the refractive index change (i.e., $\Delta n$). Then the oscillating frequency shift can be written as

$$\Delta f_{osc} = -f_{osc}\left(\frac{\Delta L}{L}+\frac{\Delta n}{n}\right) = -f_{osc}\frac{L_h}{L}\left(\alpha+\xi\right)\Delta T, \tag{29}$$

where $L_h$ is the fiber length for heating, $\alpha$ is the thermal expansion coefficient, $\xi$ is the thermo-optic coefficient, and $\Delta T$ is the temperature change. It is clear from (29) that the temperature change can be derived by measuring the frequency shift of the oscillating signals, and the sensitivity is proportional to the oscillating frequency and the ratio of $L_h/L$. In the experiment, a sensitivity of 43.91 kHz/°C was obtained within the temperature range from 20°C to 240°C, while the accuracy was calculated to be ±0.12°C [85].

Acoustic sensors using OEOs have been implemented as well [86], [87]. As shown in Fig. 10, a 1-kHz acoustic tone is directed to the fiber spool of the OEO, and the stress will induce strain in the optical fiber wound around the spool.

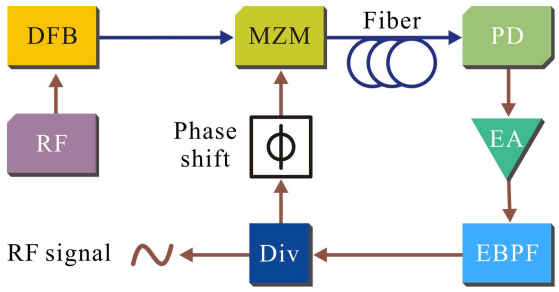


Fig. 11. OEO-based approach to the optical clock recovery. DFB, distributed feedback laser; RF, radio frequency signal; MZM, Mach–Zehnder modulator; PD, photodetector; EA, electrical amplifier; EBPF, electrical bandpass filter; Div, divider.

Then, the fiber length change (i.e., $\Delta L$) and the refractive index change (i.e., $\Delta n$) will be stimulated periodically, and the corresponding time delay variation is $\Delta\tau \approx (\Delta nL + n\Delta L)/c$. Consequently, the oscillating frequency shift is written as

$$\Delta f_{osc} = -f_{osc}\,(\Delta L/L + \Delta n/n)\,. \tag{30}$$

Therefore, the related parameters of the acoustic wave can be obtained by analyzing the oscillating frequency shift. It is noted that, due to the narrow linewidth of the high-frequency RF signal generated, OEO-based acoustic sensors can potentially provide a high spectral resolution without any cost to the sensitivity.

### *E. Optical Clock Recovery and Low-Power RF Signal Detection*

Recently, based on the oscillation gain from injection locking, OEOs have been employed for optical clock recovery and low-power RF signal detection [76], [88]–[101].

A typical scheme for optical clock recovery was released in Ref. [76], as shown in Fig. 11. An EBPF with its central frequency (i.e., $f_E$) close to the clock frequency (i.e., $f_{clock}$) is needed to carry out mode selection. On the basis of the injection locking effect presented in Section III, if $|f_E - f_{clock}|$ locates in the gain bandwidth or the locking range, the OEO system will be locked to oscillate at a single mode at $f_{clock}$. In this way, the clock signal of the optical pulses is recovered successfully. Quite a few examples have been demonstrated [88]–[97], such as the recovered optical clocks with root-mean-square (RMS) jitters of $\sim$ 40 fs @ 10 GHz, 154 fs @ $\sim$ 20 GHz, or 283 fs @ $\sim$ 40 GHz for on-off keying (OOK) signals, and 129.3 fs @ $4 \times 25$ Gb/s for differential-phase- shift-keying (DPSK) signals.

In addition to optical clock recovery, low-power RF signals buried in noise can also be detected by multi-mode OEO [98]–[101]. One of such approaches is illustrated in Fig. 12 [99], where all-optical gain is provided only by the EDFA, leading to an improvement in the sensitivity. At the mean time, no EBPF is used so that the OEO can oscillate with multiple free-running modes.

At the beginning, the intra-cavity gain is set slightly below the oscillation threshold, to be sensitive to an externally injected signal. When an incoming low-power RF signal to be detected is injected into the OEO, it will be amplified

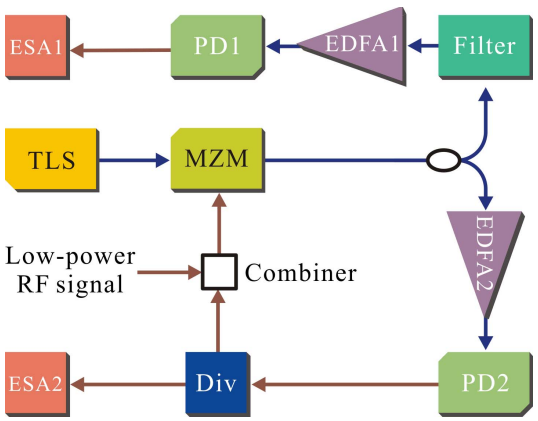


Fig. 12. Low-power RF signal detection using OEO. TLS, tunable laser source; MZM, Mach–Zehnder modulator; PD, photodetector; EDFA, Erbium doped fiber amplifier; Div, divider; ESA, electrical signal analyzer.

by the oscillation gain as its frequency locates inside the locking range of one free-running mode. While the incoming RF signal does not match the oscillating modes, only loss is offered. In this way, the low-power RF signals can be detected and the effective frequency coverage is jointly determined by the number of modes, the mode spacing, and the locking range. Experimental results demonstrate a sensitivity as low as $-83$ dBm, a mode spacing of 5.2 MHz, and a gain up to 8 dB @ $-70$ dBm, for low-power RF signals ranging from 1 to 6 GHz [99].

To enhance the detection performances, two TLSs are used to provide two sets of complementary oscillating modes [100]. The switch between the complementary modes in the OEO allows us to detect twice as many frequencies, making the detection capacity doubled. What is more, the use of semiconductor optical amplifier (SOA), rather than EDFA, minimizes the OEO loop to have a large mode spacing, such as 100 MHz.

### *F. Others: Optical Frequency Stability Measurement and Optical Power Monitoring*

In addition to examples aforementioned, OEOs have found increasing applications in other topics such as optical frequency stability measurements [102] and optical power monitoring [103].

In Ref. [102], the optical frequency stability of an LD was monitored as a Fabry-Perot etalon was used to perform mode selection in the OEO. The frequency drift of the LD is proportional to the oscillating frequency shift according to the second principle demonstrated in the Section III. Therefore, optical frequency stability can be estimated from the oscillating frequency.

For optical power monitoring [103], according to the model in Ref. [20], a relationship [see (31)] can be derived between the oscillating amplitude (i.e., $V_{osc}$) and the input optical power (i.e., $P_0$). Measuring the amplitude of the oscillating signal reveals the optical power.

$$P_0 \propto \left| \frac{V_{osc}}{J_1\,(\pi\,V_{osc}/\,V_\pi)} \right|. \tag{31}$$

TABLE I
SELECTED SPECIFICATIONS OF OEO-BASED APPROACHES

| Ref. | Target | Specifications |
|---|---|---|
| [77] | Distance/ Length change | Resolution: 1.5μm/Hz; standard deviation : 14.8 μm; length:~2km. |
| [78] | Length change | Resolution: -28kHz/cm within 10 cm range, -480kHz/cm in 2.8-cm range. |
| [79] | Distance | Maximum error: ±1.5μm; distance: 1.5 m at an emulated 3.35-km distance. |
| [80] | Refractive index | Slope: -226.62±2.53kHz/mm; uncertainty: $10^{-2}$ . |
| [81] | Refractive index | Standard deviation: less than 0.0031with 10 mm quartz cell. |
| [82] | Strain | Sensitivity: ~9.73GHz/(N/mm); resolution: $2.06\times10^{-4}$ N/mm. |
| [83] | Transverse load | Resolution: 360fm; slope: 0.20683 GHz/με; range: 0~50 με. |
| [84] | Transverse load | Sensitivity:+9.7573 GHz/(N/mm); resolution: $3.1566\times10^{-4}$ N/mm; range: ~0.6N/mm |
| [85] | Temperature | Sensitivity: 43.91 kHz/°C; accuracy: ±0.12°C ; range: 20~240 °C. |
| [86] | Acoustic tone | Spectral resolution: sub-Hz. |
| [87] | Acoustic velocity | Velocity : $(4.26\pm0.04)\times10^3$ m/s; Allan deviation of FSR: $2\times10^{-6}$. |
| [91] | Optical clock recovery | Format: RZ; locking range: ~5 kHz; RMS jitter: ~ 40 fs @ 10 GHz. |
| [92] | Optical clock recovery | Format: RZ; locking range: 37.4 MHz; RMS jitter: 283 fs @ ~ 40 GHz. |
| [94] | Optical clock recovery | Format: RZ; locking range: 360 kHz; RMS jitter: 154 fs @ ~ 20 GHz. |
| [96] | Optical clock recovery | Data rate: 4×25 Gb/s; RMS jitter: 129.3 fs for DPSK and 166.6 fs for OOK. |
| [98] | Low-power RF signal detection | Frequency range: ~2 GHz; mode spacing: ~400 MHz; sensitivity: -75 dBm; gain:10 dB |
| [99] | Low-power RF signal detection | Frequency range: 1~ 6 GHz; mode spacing: 5.2 MHz; sensitivity: -83 dBm; gain: up to 8 dB @ -70 dBm. |
| [100] | Low-power RF signal detection | Sensitivity: -78.4dBm; mode spacing: 100MHz; gain bandwidth: 140 MHz. |
| [102] | Optical frequency stability | Frequency resolution: ~3.5kHz; range: 5 MHz; update rates: 90 Hz |
| [103] | Optical power monitoring | Dynamic range: 6dB; accuracy: 0.25dB. |
| This paper | Position finding | Sensitivity: 254.66 kHz/cm; range: 0~3 cm. |

A sub-conclusion is drawn here for this overall review to diverse applications. An X-to-frequency mapping or relationship is firstly established from the three operation principles. Then, an analysis of the oscillating frequency or/and the FSR is capable of obtaining the target parameter or signal, such as distance, length change, refractive index, temperature, low-power RF signal, and optical clock. These emerging OEO-based approaches to sensing, measurement and detection have the advantages of high resolution and high SNR, while some selected specifications are listed in Table I.

## V. NOVEL APPLICATION EXAMPLE: POSITION FINDING USING OEO

After the overall review in Section IV, a novel application to in-line position finding using OEO is proposed and experimentally demonstrated for the first time in this section.

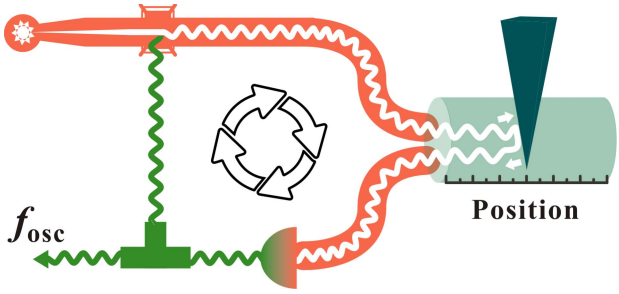


Fig. 13. Conceptual diagram of the proposed OEO-based position-finding approach.

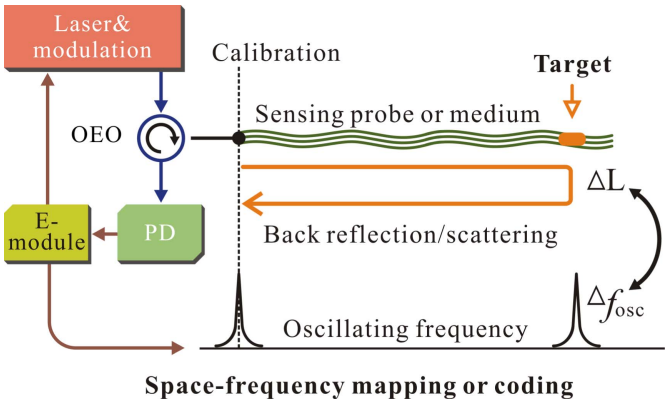


Fig. 14. Generic architecture to the OEO-based position-finding approach and the space-frequency coding behind this approach. PD, photodetector; OEO, optoelectronic oscillator.

### A. Design and Principle

The conceptual diagram and the generic architecture of the proposed approach are shown in Figs. 13 and 14, respectively. The OEO is simply comprised of a laser and modulation module, a PD, and an E-Module including electrical filter, amplifier, and divider. A sensing probe or medium is inserted into the loop by using an optical circulator. When the target position along the sensing medium is affected by environmental factors (e.g., heat or strain), a backward reflection or scattering of the optical signal will be stimulated to provide feedback for initiating an oscillation. Potential elements or schemes to form backward reflection or scattering include, but not limited to, FBG, Rayleigh scattering, Brillouin scattering, strain, bending, radiation, and heating.

To find the target position, we firstly set a reference as the calibration position, and the corresponding total length (say $L_0$) of the OEO loop is already given. According to the calibration position, the oscillating frequency corresponding to the target position is derived as

$$f_{osc} = f_0 + \frac{kc}{L_0 + 2n\Delta L}, \tag{32}$$

where $f_0$ is related to the bias of the MZM [20], [98], $k$ represents the order of the oscillating mode, $n$ is the refractive index of sensing medium, and $\Delta L$ is the spatial distance between calibration and target positions. Assuming $L_0 \gg 2n\Delta L$, the oscillating frequency shift with respective to the

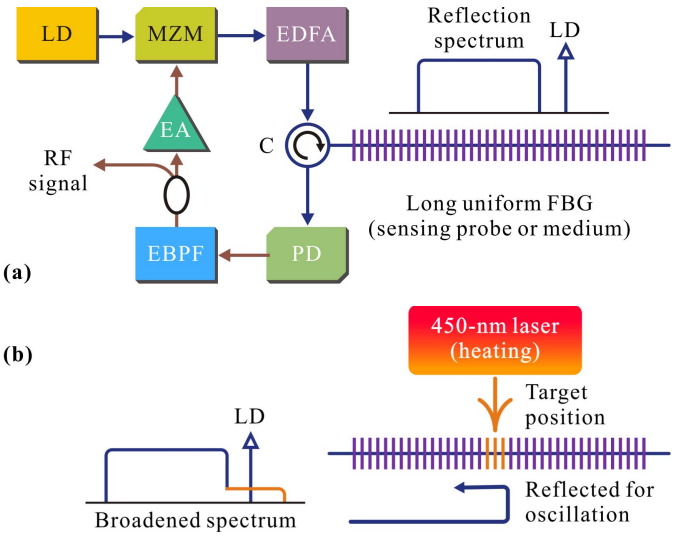


Fig. 15. (a) Block diagram of the OEO-based position-finding approach using a long uniform FBG and the original reflection spectrum without heating; (b) illustration of local heating to the long FBG and the resulting reflection spectrum broadening. LD, laser diode; MZM, Mach–Zehnder modulator; EDFA, Erbium doped fiber amplifier; PD, photodetector, EBPF, electrical bandpass filter; EA, electrical amplifier; C, optical circulator; FBG, fiber Bragg grating.

calibration position can be expressed as

$$\Delta f_{osc} = -2nkc\frac{\Delta L}{L_0^2}. \tag{33}$$

Consequently, the target position in terms of the spatial distance to the calibration position can be derived as

$$\Delta L = -\frac{L_0^2}{2nkc}\Delta f_{osc}. \tag{34}$$

It is clear that (34) reveals a linear relationship between the spatial position and the oscillating frequency shift for position finding. This is just the operation principle behind this approach, and we define it as "space-to-frequency mapping or coding", as illustrated in Fig. 14. Usually, a narrow EBPF is used to provide a single-mode oscillation in this approach, such that $f_0$ and $k$ can be determined in accordance with the calibration position.

Since $f_{osc}$ or $\Delta f_{osc}$ can be simply obtained by using an electrical spectrum analyzer, the target position being affected by local environmental parameters can be effectively measured. Owing to the available high-resolution frequency analysis in the electrical domain, high resolution can be ensured for position finding.

A detailed setup for this position-finding approach is designed and shown in Fig. 15, where a long FBG acts as the sensing medium. The optical carrier emitted from the LD is modulated by an RF signal, then sent to the FBG through the optical circulator. As shown in Fig. 15(a), the wavelength of the optical carrier is placed out of the reflection bandwidth of the FBG. In this case, no optical signal will circle to the PD to sustain an oscillation. On the other hand, if any environmental influence (e.g., pressure, temperature, or strain) is applied to a local segment of the FBG, the reflection spectrum will be broadened towards long wavelength range. Consequently, as illustrated in Fig. 15(b), the modulated optical signal is reflected back to the PD. As the reflected power and the in-loop gain are large enough, a sustainable oscillation will be established and the frequency of the oscillating signal indicates the target position being stimulated.

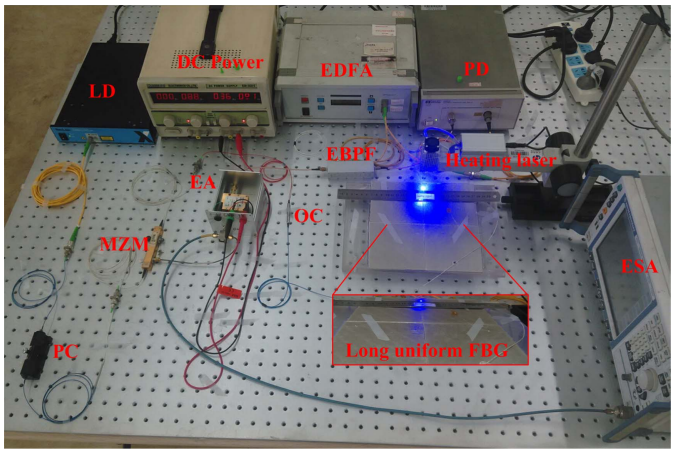


Fig. 16. Experiment setup of the position finding approach using a long uniform FBG.

### B. Experiments and Results

To support the proposed approach, experiments are performed with the setup shown in Fig. 16. A 3-cm uniform FBG is used in our experiments as the sensing medium. As illustrated in Fig. 15(a), we firstly place the optical carrier out of the reflection band of the FBG at the long-wavelength direction, so that no oscillation will occur.

Then a 450-nm laser source is used to locally heat a specific position of the FBG, serving as an environmental perturbation to a target position. Due to the thermo-optic effect, the reflection spectrum of the heating position will move towards long wavelength, while the reflection spectra of other positions keep unchanged. As a result, the whole reflection spectrum will be broadened to cover the optical carrier with low reflectivity, and the OEO loop is prolonged by a length twice the relative distance between the calibration position and the heating position. In this way, oscillation will occur and the oscillating frequency indicates the exact position being locally heated.

In addition, to ensure single-mode operation without mode hopping, the EBPF used in our experiment has an ultra-narrow bandwidth of 1 MHz, while the mode spacing of the OEO is estimated to be 7 MHz.

For simplicity of comparison, the reflection spectra of FBG before and after heating are depicted in Fig. 17, respectively. The central wavelength of the reflection spectrum is 1551.38 nm, so the optical carrier at 1551.72 nm is totally out of the reflection band of the FBG. After heating, a broadening on the reflection spectrum towards long wavelength is observed. Thanks to this spectrum broadening, the optical carrier is reflected back to the PD to sustain a continuous oscillation.

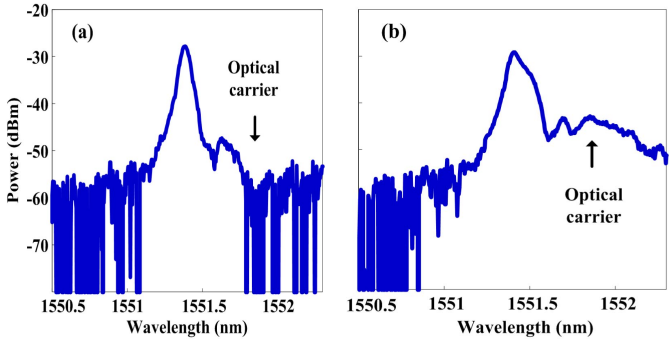


Fig. 17. Reflection spectra of the FBG before (a) and after (b) being heated by the 450-nm laser.

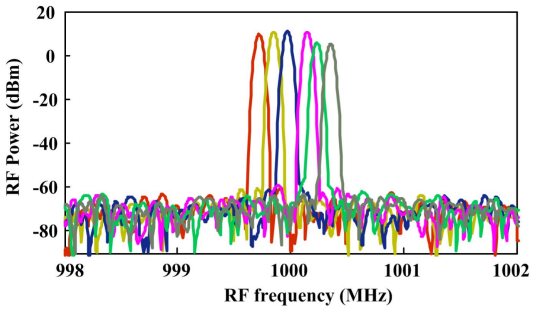


Fig. 18. Electrical spectra of oscillating signals generated at different target positions heated.

During the experiments, the beam of the heating laser is moved with a step of 0.5 cm to emulate different target positions. Thus, different RF oscillating frequencies are obtained for different local positions being heated, as shown in Fig. 18. It can be seen that the corresponding oscillating frequency changes with the move of the target position heated, without any ambiguity. Quantitatively, a linear relationship between the oscillating frequency and the target position heated yields and the measurement sensitivity is 254.66 kHz/cm within the range of 0∼3 cm, as shown in Fig. 19. Note that higher measurement sensitivity can be easily reached by selecting high-order oscillating mode using high-frequency EBPF. Also, the accuracy or the stability can be improved by using additional feedback control shown in next section, with undesired environmental interferences reduced.

In addition, besides the long FBGs used here, it should be pointed out that other optical element or schemes can also be used as sensing mediums for the proposed approach. As long as the backward reflection or scattering from the target position along the optical link is large enough for sustaining an oscillation and no reflection or scattering from other positions, we are capable of linking the oscillating frequency with the target position according to "space-to-frequency mapping or coding" shown in Fig. 14.

## VI. Calibration and Stabilization

For all applications to sensing, measurement and detection, the calibration and the stability of OEOs are always a critical step to ensure reliability and accuracy. For instance, a stable

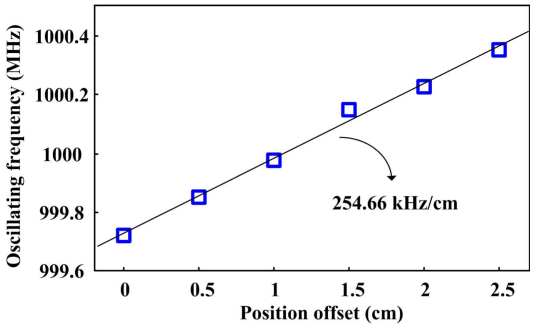


Fig. 19. Variation of RF oscillating frequency versus the target position heated with respective to the calibration position (zero offset). The calibration point is placed at the far end of the FBG in the experiment, not at the near end in Fig. 14.

reference oscillator can effectively circumvent the influence of undesired frequency shifts resulted from temperature change or vibration [79]. In this section, we will briefly introduce methods commonly used to improve the stability of OEOs, which are classified into three categories, injection locking or coupled OEOs [34], [104]–[113], PLL technique [112], [114]–[117], and Pound-Drever-Hall (PDH) technique [37], [118]–[121].

### A. Injection Locking or Coupled OEOs

Injection locking can provide an effective solution to improve the stability of OEOs. In the case of single injection, the oscillating frequency is locked to a high-quality electrical/optical reference signal, and the stability of the OEO is directly determined by the reference signal. As for mutual injection, one OEO and the second oscillator (e.g., the other OEO [106] or fiber ring laser [107]–[113]) operate at the same oscillating frequency. One harmonic of the OEO is locked to one harmonic of the second oscillator, such that their oscillating frequencies mutually restrict and refine. Correspondingly, a self-stabilization system will be established. In some scenarios, the system using mutual injection is also defined as coupled OEOs.

### B. PLL Technique

Basically, the PLL technique is mostly used to lock the frequency or the phase of the signal to a low-frequency stable signal or oscillator. With the same architecture, the PLL can also be introduced for stabilizing the operation of OEOs. By comparing the oscillating signal of the OEO to a reference signal, a correction or feedback signal is generated and sent back to feedback control units. Then, the parameters of the OEO system can be dynamically adjusted by feedback control units, such as the voltage-controlled RF phase/frequency shifter [114], [115], the voltage controlled optical phase shifter/cavity-length control module [112], [116] and the bias of the MZM [117]. Correspondingly, the oscillation of OEO is stabilized further.

### C. PDH Technique

As well known, the PDH technique is a powerful tool to lock an LD with an optical resonator. Likewise, the PDH is capable

of improving the frequency stability of the OEOs where an optical resonator is used for mode selection.

In general, the relative drift between the wavelengths of the LD and of the optical resonator is converted into the deviation on the oscillating frequency of OEOs. To fix this problem, the wavelength of the LD should be locked to one peak of the optical resonator, and the procedure is listed as follows. The optical signal from the LD is firstly frequency modulated by a low-frequency tone, and sent to the optical resonator. The intensity of the reflected optical signal discriminates the relative offset between the wavelength of the LD and the specific peak of the optical resonator. In particular, the derivative of the reflected intensity clarifies a positive or negative offset with respective to the resonant peak, according to the in-phase or out-of-phase variation [118], [120]. Thus, both the value and the direction of the relative offset are used as feedback for active stabilization to the LD, making the wavelength of the LD closely locked to the optical resonator. As an example, the fractional frequency stability of the OEO was improved to $3.3 \times 10^{-10}$ @10.5GHz at 1-s offset by using the PDH technique [120].

## VII. Discussions on Features and Future Prospects

After these diverse applications and examples above, distinct features and future prospects for OEO-based sensing, measurement, and detection are discussed in this section.

### A. Features in Frequency Resolution and Signal-to-Noise Ratio

During the procedure of sensing, measurements, and detection, the oscillating frequency of OEOs is evaluated in the electrical domain to measure the target parameter or signal. Therefore, distinct features of such solutions lie in fine frequency resolution and high SNR, owing to the intrinsic ultra-low phase noise or pure spectrum of oscillating signals in OEOs. On the other hand, the measurement range of such solutions is usually limited by FSR or mode spacing. To circumvent this issue, additional measurements into the mode order or the fundamental frequency are needed [79].

To clarify the distinct features, we start with the phase noise performance of OEOs estimated in many papers [122]–[124]. Like in electronic oscillators where the specifications are determined by phase noise, the frequency resolution is limited by the "close-in" phase noise and the SNR is mostly determined by the "white" phase noise in OEOs. According to the phase noise in terms of power-law spectral density presented in Ref. [123], the frequency resolution can be sub-Hz with respective to an extremely low linewidth. Meanwhile, from the phase noise, the power of in-band noise (i.e., $P_{noise}$) relative to the carrier can be derived via an integral:

$$P_{noise} = \int_{f_{\min}}^{f_{\max}} S_{\varphi}(f) df, \tag{35}$$

where $S_{\varphi}(f)$ is the single-sideband power spectral density, $f_{\min}$ and $f_{\max}$ are the lower and the upper boundaries of the integral, respectively. As a compact example, the total noise can be approximately calculated from the phase noise released in Ref. [123], and the SNR is derived as high as 50 dB within a 1-MHz bandwidth.

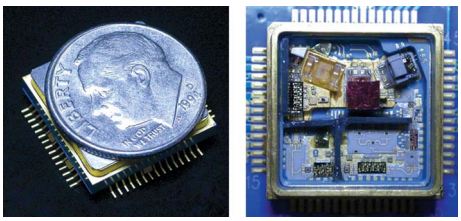

Fig. 20. Photograph of miniature OEOs using WGMR released by OEWave (reprinted from Ref. [22] with copyright permission).

While in other techniques, such as optical frequency- or time-domain refrectometry (OFDR or OTDR), the resultant SNRs for demodulation are usually limited. For examples, as far as we know, SNRs less than 20 dB were obtained for phase sensitive OTDR [125], [126], and SNRs (defined as sidelobe suppression ratio [127], [128]) up to 34 dB for OFDR, after specific compensation, coding, or amplification.

### B. Future Prospects

Among the diverse applications and examples aforementioned, it is obvious that most OEOs are implemented by using discrete, bulky devices recently, such as commercially available tunable laser modules/kits and external electro-optic modulators. However, ever-increasing concerns come in front of both academic and industry communities to strive for compact size, light weight, low power consumption, high reliability, and low cost, to create niche scenarios and to facilitate innovative applications in medicine, communications, radar, electronic warfare, and space exploration.

Fortunately, such miniature OEOs are already commercially available, e.g., the products released by OEwave in United States. By using a high-Q WGMR, a packaged product is smaller than a coin [22], as shown in Fig. 20. The exact size is $0.6 \times 0.6 \times 0.15$ inch and the available phase noise is $-108$ dBc/Hz @10 kHz for an oscillating tone at 35 GHz [129]. Recently, ultra-high-Q silica disk resonator was employed to construct oscillators, and the size is only $\sim$5 or 6 mm [130]–[132]. Such an on-chip Brillouin oscillator demonstrates a record low electronic white-phase-noise floor (i.e., $-160$ dBc/Hz [131]) or an ultra-low phase noise (i.e., $-170$ dBc/Hz@10 MHz offset [132]) for microcavity-based microwave sources. More details about compact high-Q WGMRs can be found in Ref. [133].

On the other hand, there is still a long way to go for further cutting the size and the power consumption of OEOs and much effort is exceedingly needed, along with the rapid development of photonic integrated circuits (PICs). As summarized in several review or tutorial papers, several leading platforms are being developed to demonstrate photonic or hybrid integrated functional devices or systems [134]–[145], such as InP, silica planar lightwave circuits, silicon-on-insulator (SOI), and $Si_3N_4/SiO_2$. Multiple tunable LDs, modulators, amplifiers, waveguides, and PDs can

be integrated in a monolithic chip with a size of millimeter. Thus, in the near future, OEOs towards sensing, measurement, and detection applications will be fabricated in a scale of millimeter, sub-millimeter, or even smaller, facilitating both traditional and prospective applications.

## VIII. Conclusion

In conclusion, as emerging applications of OEOs, principles and advances regarding sensing, measurement, and detection were reviewed and summarized, including the analytical model and three key operation principles. According to the three principles, a host of OEO-based approaches were demonstrated, showing versatile, powerful functionalities and excellent specifications in the fields of sensing, measurement, and detection. As a new application, a novel approach using OEO for position finding was proposed, and a measurement sensitivity of 254.66 kHz/cm was obtained in experiment. Finally, calibration and stabilization solutions for improving the performances of OEO-based approaches were introduced, followed by future trends and prospects in compact and integrated OEOs for achieving small footprint, light weight, low power consumption, and high reliability. It is extremely desired that miniature and versatile OEOs will offer distinct specifications and create numerous niche applications in medicine, metrology, communications, radar, electronic warfare, satellite and space exploration, and civil engineering in the near future.

## Acknowledgment

X. Zou would like to thank Prof. Jianping Yao (University of Ottawa, Canada) and Prof. Andreas Stöhr (University of Duisburg-Essen, Germany) for supports and helps.

## References

[1] S. H. Strogatz, *SYNC: The Emerging Science of Spontaneous Order*. New York, NY, USA: Theia, 2003.

[2] *Oscillation*, [Online]. Available: https://en.wikipedia.org/wiki/Oscillation, accessed September 15, 2015.

[3] J. Weber, "Quantum theory of a damped electrical oscillator and noise," *Phys. Rev.*, vol. 90, no. 5, pp. 977–982, Jun. 1953.

[4] J. P. Gordon, H. J. Zeiger, and C. H. Townes, "The maser—New type of microwave amplifier, frequency standard, and spectrometer," *Phys. Rev.*, vol. 99, p. 1264, Aug. 1955.

[5] T. H. Maiman, "Stimulated optical radiation in Ruby," *Nature*, vol. 187, no. 4736, pp. 493–494, Aug. 1960.

[6] U. Fano and J. W. Cooper, "Spectral distribution of atomic oscillator strengths," *Rev. Mod. Phys.*, vol. 40, no. 3, pp. 441–507, Jul. 1968.

[7] Y. Fukuda *et al.*, "Evidence for oscillation of atmospheric neutrinos," *Phys. Rev. Lett.*, vol. 81, no. 8, pp. 1562–1567, Aug. 1998.

[8] E. Thomson, "Method of and means for producing alternating currents," U.S. Patent 500 630, Jul. 4, 1893.

[9] F. Dearborn, C. Hempstead, and W. E. Worthington, Eds., *Encyclopedia of 20th-Century Technology*, vol. 2. New York, NY, USA: Routledge, Jan. 2005.

[10] R. T. Kersten, "Ein optisches Nachrichtensystem mit Bauelementen der integrierten Optik für die Übertragung hoher Bitraten," *Arch. Elektrotech.*, vol. 60, no. 6, pp. 353–359, Nov. 1978.

[11] H. F. Schlaak, A. Neyer, and W. Sohler, "Electrooptical oscillator using an integrated cutoff modulator," *Opt. Commun.*, vol. 32, no. 1, pp. 72–74, Jan. 1980.

[12] T. C. Damen and M. A. Duguay, "Optoelectronic regenerative pulser," *Electron. Lett.*, vol. 16, no. 5, pp. 166–167, Feb. 1980.

[13] W. Sohler, "Optical bistable device as electro-optical multivibrator," *Appl. Phys. Lett.*, vol. 36, no. 5, pp. 351–383, Mar. 1980.

[14] H. F. Schlaak and R. T. Kersten, "Integrated optical oscillators and their applications to optical communication systems," *Opt. Commun.*, vol. 36, no. 3, pp. 186–188, Feb. 1981.

[15] M. Nakazawa, M. Tokuda, and N. Uchida, "Self-sustained intensity oscillation of a laser diode introduced by a delayed electrical feedback using an optical fiber and an electrical amplifier," *Appl. Phys. Lett.*, vol. 39, no. 5, pp. 379–381, Sep. 1981.

[16] A. Neyer and E. Voges, "High-frequency electro-optic oscillator using an integrated interferometer," *Appl. Phys. Lett.*, vol. 40, no. 1, pp. 6–8, Jan. 1982.

[17] A. Neyer and E. Voges, "Nonlinear electrooptic oscillator using an integrated interferometer," *Opt. Commun.*, vol. 37, no. 3, pp. 169–174, May 1982.

[18] M. F. Lewis, "Novel RF oscillator using optical components," *Electron. Lett.*, vol. 28, no. 1, pp. 31–32, Jan. 1992.

[19] X. S. Yao and L. Maleki, "High frequency optical subcarrier generator," *Electron. Lett.*, vol. 30, no. 18, pp. 1525–1526, Sep. 1994.

[20] X. S. Yao and L. Maleki, "Optoelectronic microwave oscillator," *J. Opt. Soc. Amer. B*, vol. 13, no. 8, pp. 1725–1735, Aug. 1996.

[21] X. S. Yao and L. Maleki, "Converting light into spectrally pure microwave oscillation," *Opt. Lett.*, vol. 21, no. 7, pp. 483–485, Apr. 1996.

[22] L. Maleki, "Sources: The optoelectronic oscillator," *Nature Photon.*, vol. 5, no. 12, pp. 728–730, Dec. 2011.

[23] T. Berceli and P. R. Herczfeld, "Microwave photonics—A historical perspective," *IEEE Trans. Microw. Theory Techn.*, vol. 58, no. 11, pp. 2992–3000, Nov. 2010.

[24] L. Maleki, "The opto-electronic oscillator (OEO): Review and recent progress," in *Proc. Eur. Freq. Time Forum*, Gothenburg, Sweden, Apr. 2012, pp. 497–500.

[25] M. E. Belkin and A. V. Loparev, "A microwave optoelectronic oscillator: Mach–Zehnder modulator or VCSEL based layout comparison," in *Proc. PIERS*, Moscow, Russia, Aug. 2012, pp. 1138–1142.

[26] X. S. Yao and L. Maleki, "Multiloop optoelectronic oscillator," *IEEE J. Quantum Electron.*, vol. 36, no. 1, pp. 79–84, Jan. 2000.

[27] T. Bánky, B. Horváth, and T. Berceli, "Optimum configuration of multiloop optoelectronic oscillators," *J. Opt. Soc. Amer. B*, vol. 23, no. 7, pp. 1371–1380, 2006.

[28] T. Berceli, T. Bánky, and B. Horváth, "Opto-electronic generation of stable and low noise microwave signals," *IEE Proc.-Optoelectron.*, vol. 153, no. 3, pp. 119–127, Jun. 2006.

[29] J. Yang, Y. Jin-Long, W. Yao-Tian, Z. Li-Tai, and Y. En-Ze, "An optical domain combined dual-loop optoelectronic oscillator," *IEEE Photon. Technol. Lett.*, vol. 19, no. 11, pp. 807–809, Jun. 1, 2007.

[30] E. Shumakher and G. Eisenstein, "A novel multiloop optoelectronic oscillator," *IEEE Photon. Technol. Lett.*, vol. 22, no. 20, pp. 1881–1883, Nov. 15, 2008.

[31] L. Maleki, D. Eliyahu, and V. Ilchenko, "Tunable multi-loop optoelectronic oscillator with tunable RF or microwave filter based on optical filtering," U.S. Patent, 7 460 746, Dec. 2, 2008.

[32] X. Liu, W. Pan, X. Zou, B. Luo, L. Yan, and B. Lu, "A reconfigurable optoelectronic oscillator based on cascaded coherence-controllable recirculating delay lines," *Opt. Exp.*, vol. 20, no. 12, pp. 13296–13301, Jun. 2012.

[33] S. Jia *et al.*, "A novel optoelectronic oscillator based on wavelength multiplexing," *IEEE Photon. Technol. Lett.*, vol. 27, no. 2, pp. 213–216, Jan. 15, 2014.

[34] W. Zhou and G. Blasche, "Injection-locked dual opto-electronic oscillator with ultra-low phase noise and ultra-low spurious level," *IEEE Trans. Microw. Theory Techn.*, vol. 53, no. 3, pp. 929–933, Mar. 2005.

[35] H. Tavernier *et al.*, "Optical disk resonator with microwave free spectral range for optoelectronic oscillator," in *Proc. 22nd Eur. Time Freq. Forum*, Toulouse, France, Apr. 2008, paper FPE-0179, pp. 1–6.

[36] P. S. Devgan, V. J. Urick, J. F. Diehl, and K. J. Williams, "Improvement in the phase noise of a 10 GHz optoelectronic oscillator using all-photonic gain," *J. Lightw. Technol.*, vol. 27, no. 15, pp. 3189–3193, Aug. 1, 2009.

[37] J. M. Kim and D. Cho, "Optoelectronic oscillator stabilized to an intra-loop Fabry–Perot cavity by a dual servo system," *Opt. Exp.*, vol. 18, no. 14, pp. 14905–14912, Jul. 2010.

[38] I. Ozdur, M. Akbulut, N. Hoghooghi, D. Mandridis, M. U. Piracha, and P. J. Delfyett, "Optoelectronic loop design with 1000 finesse Fabry–Perot etalon," *Opt. Lett.*, vol. 35, no. 6, pp. 799–801, Mar. 2010.

[39] A. B. Matsko, D. Eliyahu, and L. Maleki, "Theory of coupled opto-electronic microwave oscillator II: Phase noise," *J. Opt. Soc. Amer. B*, vol. 30, no. 12, pp. 3316–3323, Dec. 2013.

[40] Y. Mei, T. Jin, H. Chi, S. Zheng, X. Jin, and X. Zhang, "Optoelectronic oscillator with phase-shifted fiber Bragg grating," *Opt. Commun.*, vol. 319, pp. 117–120, May 2014.

[41] T. Sakamoto, T. Kawanishi, and M. Izutsu, "Optoelectronic oscillator using push-pull Mach–Zehnder modulator biased at null point for optical two-tone signal generation," in *Proc. Conf. Lasers Electro-Opt.*, Baltimore, MD, USA, May 2005, pp. 877–879.

[42] M. Shin and P. Kumar, "Optical microwave frequency up-conversion via a frequency-doubling optoelectronic oscillator," *IEEE Photon. Technol. Lett.*, vol. 19, no. 21, pp. 1726–1728, Nov. 1, 2007.

[43] S. Pan and J. Yao, "A frequency-doubling optoelectronic oscillator using a polarization modulator," *IEEE Photon. Technol. Lett.*, vol. 21, no. 13, pp. 929–931, Jul. 1, 2009.

[44] L. Wang, N. Zhu, W. Li, and J. Liu, "A frequency-doubling optoelectronic oscillator based on a dual-parallel Mach–Zehnder modulator and a chirped fiber Bragg grating," *IEEE Photon. Technol. Lett.*, vol. 23, no. 22, pp. 1688–1690, Nov. 15, 2011.

[45] W. Li and J. Yao, "Optically tunable frequency-multiplying optoelectronic oscillator," *IEEE Photon. Technol. Lett.*, vol. 24, no. 10, pp. 812–814, May 15, 2012.

[46] B. Yang *et al.*, "Optically tunable frequency-doubling Brillouin optoelectronic oscillator with carrier phase-shifted double sideband modulation," *IEEE Photon. Technol. Lett.*, vol. 24, no. 12, pp. 1051–1053, Jun. 15, 2012.

[47] D. Zhu, S. Pan, and D. Ben, "Tunable frequency-quadrupling dual-loop optoelectronic oscillator," *IEEE Photon. Technol. Lett.*, vol. 24, no. 3, pp. 194–196, Feb. 1, 2011.

[48] X. Liu, W. Pan, X. Zou, D. Zheng, L. Yan, and B. Luo, "Frequency-doubling optoelectronic oscillator using DSB-SC modulation and carrier recovery based on stimulated Brillouin scattering," *IEEE Photon. J.*, vol. 5, no. 2, Apr. 2013, Art. ID 6600606.

[49] W. Li and J. Yao, "An optically tunable optoelectronic oscillator," *J. Lightw. Technol.*, vol. 28, no. 18, pp. 2640–2645, Sep. 15, 2010.

[50] S. Pan and J. Yao, "Wideband and frequency-tunable microwave generation using an optoelectronic oscillator incorporating a Fabry–Perot laser diode with external optical injection," *Opt. Lett.*, vol. 35, no. 11, pp. 1911–1913, Jun. 2010.

[51] W. Li and J. Yao, "A wideband frequency tunable optoelectronic oscillator incorporating a tunable microwave photonic filter based on phase-modulation to intensity-modulation conversion using a phase-shifted fiber Bragg grating," *IEEE Trans. Microw. Theory Techn.*, vol. 60, no. 6, pp. 1735–1742, Jun. 2012.

[52] M. Li, W. Li, and J. Yao, "Tunable optoelectronic oscillator incorporating a high-$Q$ spectrum-sliced photonic microwave transversal filter," *IEEE Photon. Technol. Lett.*, vol. 24, no. 14, pp. 1251–1253, Jul. 15, 2012.

[53] F. Jiang *et al.*, "An optically tunable wideband optoelectronic oscillator based on a bandpass microwave photonic filter," *Opt. Exp.*, vol. 21, no. 14, pp. 16381–16389, Jul. 2013.

[54] X. Xie *et al.*, "Wideband tunable optoelectronic oscillator based on a phase modulator and a tunable optical filter," *Opt. Lett.*, vol. 38, no. 5, pp. 655–657, Mar. 2013.

[55] Y. K. Chembo, L. Larger, H. Tavernier, R. Bendoula, E. Rubiola, and P. Colet, "Dynamic instabilities of microwaves generated with optoelectronic oscillators," *Opt. Lett.*, vol. 32, pp. 2571–2573, Sep. 2007.

[56] Y. K. Chembo, L. Larger, and P. Colet, "Nonlinear dynamics and spectral stability of optoelectronic microwave oscillators," *IEEE J. Quantum Electron.*, vol. 44, no. 9, pp. 858–866, Sep. 2008.

[57] K. E. Callan, L. Illing, Z. Gao, D. J. Gauthier, and E. Schöll, "Broadband chaos generated by an optoelectronic oscillator," *Phys. Rev. Lett.*, vol. 104, no. 11, p. 113901, Mar. 2010.

[58] L. Larger and J. M. Dudley, "Nonlinear dynamics: Optoelectronic chaos," *Nature*, vol. 465, pp. 41–42, May 2010.

[59] J. Zheng *et al.*, "Spectral sculpting of chaotic-UWB signals using a dual-loop optoelectronic oscillator," *IEEE Photon. Technol. Lett.*, vol. 25, no. 24, pp. 2397–2400, Dec. 15, 2013.

[60] W. Li, F. Kong, and J. Yao, "Arbitrary microwave waveform generation based on a tunable optoelectronic oscillator," *J. Lightw. Technol.*, vol. 31, no. 23, pp. 3780–3786, Dec. 1, 2013.

[61] W. Li and J. Yao, "Generation of linearly chirped microwave waveform with an increased time-bandwidth product based on a tunable optoelectronic oscillator and a recirculating phase modulation loop," *J. Lightw. Technol.*, vol. 32, no. 20, pp. 3573–3579, Oct. 15, 2014.

[62] W. Y. Wang, W. Li, W. H. Sun, W. Wang, J. G. Liu, and N. H. Zhu, "Triangular microwave waveforms generation based on an optoelectronic oscillator," *IEEE Photon. Technol. Lett.*, vol. 27, no. 5, pp. 522–525, Mar. 1, 2015.

[63] J. Lasri *et al.*, "A self-starting hybrid optoelectronic oscillator generating ultra low jitter 10-GHz optical pulses and low phase noise electrical signals," *IEEE Photon. Technol. Lett.*, vol. 14, no. 7, pp. 1004–1006, Jul. 2002.

[64] P. Devgan, D. Serkland, G. Keeler, K. Geib, and P. Kumar, "An optoelectronic oscillator using an 850-nm VCSEL for generating low jitter optical pulses," *IEEE Photon. Technol. Lett.*, vol. 18, no. 5, pp. 685–687, Mar. 1, 2006.

[65] Y. Jiang, J.-L. Yu, H. Hu, W.-R. Wang, Y.-T. Wang, and E.-Z. Yang, "Phase-modulator-based optoelectronic oscillator for generating short optical pulse and microwave signal," *Opt. Eng.*, vol. 46, no. 9, p. 090502, Sep. 2007.

[66] Y. K. Chembo, A. Hmima, P.-A. Lacourt, L. Larger, and J. M. Dudley, "Generation of ultralow jitter optical pulses using optoelectronic oscillators with time-lens soliton-assisted compression," *J. Lightw. Technol.*, vol. 27, no. 22, pp. 5160–5167, Nov. 15, 2009.

[67] Y.-C. Chi and G.-R. Lin, "A self-started laser diode pulsation based synthesizer-free optical return-to-zero on–off-keying data generator," *IEEE Trans. Microw. Theory Techn.*, vol. 58, no. 8, pp. 2292–2298, Aug. 2010.

[68] K. Koizumi, M. Yoshida, and M. Nakazawa, "A 10-GHz optoelectronic oscillator at 1.1 $\mu$m using a single-mode VCSEL and a photonic crystal fiber," *IEEE Photon. Technol. Lett.*, vol. 22, no. 5, pp. 293–295, Mar. 1, 2010.

[69] H. Hasegawa, "Optoelectronic oscillator and pulse generator," U.S. Patent 8 031 012 B2, Oct. 4, 2011.

[70] A. Sherman and M. Horowitz, "Ultralow-repetition-rate pulses with ultralow jitter generated by passive mode-locking of an optoelectronic oscillator," *J. Opt. Soc. Amer. B*, vol. 30, no. 11, pp. 2980–2983, Nov. 2013.

[71] N. Huang, M. Li, Y. Deng, and N. H. Zhu, "Optical pulse generation based on an optoelectronic oscillator with cascaded nonlinear semiconductor optical amplifiers," *IEEE Photon. J.*, vol. 6, no. 1, Feb. 2014, Art. ID 5500208.

[72] T. Sakamoto, T. Kawanishi, and M. Izutsu, "Optoelectronic oscillator using a $LiNbO_3$ phase modulator for self-oscillating frequency comb generation," *Opt. Lett.*, vol. 31, no. 6, pp. 811–813, Mar. 2006.

[73] W. Li, W. T. Wang, W. H. Sun, L. Wang, J. G. Liu, and N. H. Zhu, "Generation of flat optical frequency comb using a single polarization modulator and a Brillouin-assisted power equalizer," *IEEE Photon. J.*, vol. 6, no. 2, Apr. 2014, Art. ID 7900908.

[74] X. Xie *et al.*, "Low-noise and broadband optical frequency comb generation based on an optoelectronic oscillator," *Opt. Lett.*, vol. 39, no. 4, pp. 785–788, Feb. 2014.

[75] X. Liu, W. Pan, X. Zou, L. Yan, B. Luo, and B. Lu, "Investigation on tunable modulation index in the polarization-modulator-based optoelectronic oscillator," *IEEE J. Quantum Electron.*, vol. 50, no. 2, pp. 68–73, Feb. 2014.

[76] L. Huo, Y. Dong, C. Lou, and Y. Gao, "Clock extraction using an optoelectronic oscillator from high-speed NRZ signal and NRZ-to-RZ format transformation," *IEEE Photon. Technol. Lett.*, vol. 15, no. 7, pp. 981–983, Jul. 2003.

[77] T. Zhang, J. Zhu, T. Guo, J. Wang, and S. Ye, "Improving accuracy of distance measurements based on an optoelectronic oscillator by measuring variation of fiber delay," *Appl. Opt.*, vol. 52, no. 15, pp. 3495–3499, May 2013.

[78] X. Zou, M. Li, W. Pan, B. Luo, L. Yan, and L. Shao, "Optical length change measurement via RF frequency shift analysis of incoherent light source based optoelectronic oscillator," *Opt. Exp.*, vol. 22, no. 9, pp. 11129–11139, May 2014.

[79] J. Wang *et al.*, "Long-range, high-precision absolute distance measurement based on two optoelectronic oscillators," *Opt. Lett.*, vol. 39, no. 15, pp. 4412–4415, Aug. 2014.

[80] L. D. Nguyen, K. Nakatani, and B. Journet, "Refractive index measurement by using an optoelectronic oscillator," *IEEE Photon. Technol. Lett.*, vol. 22, no. 12, pp. 857–859, Jun. 15, 2010.

[81] T. T. Pham, I. Ledoux-Rak, B. Journet, and V. Y. Vu, "A study on measuring refractive index by using an optoelectronic oscillator," in *Proc. IEEE 5th Int. Conf. Commun. Electron.*, Danang, Bietnam, Jul./Aug. 2014, pp. 17–22.

[82] M. Li, W. Li, J. Yao, and J. Azaña, "Femtometer-resolution wavelength interrogation using an optoelectronic oscillator," in *Proc. IEEE Photon. Conf.*, Burlingame, CA, USA, Sep. 2012, pp. 298–299.

[83] F. Kong, W. Li, and J. Yao, "Transverse load sensing based on a dual-frequency optoelectronic oscillator," *Opt. Lett.*, vol. 38, no. 14, pp. 2611–2613, Jul. 2013.

[84] F. Kong, B. Romeira, J. Zhang, W. Li, and J. Yao, "A dual-wavelength fiber ring laser incorporating an injection-coupled optoelectronic oscillator and its application to transverse load sensing," *J. Lightw. Technol.*, vol. 32, no. 9, pp. 1784–1793, May 1, 2014.

[85] Y. Zhu, X. Jin, H. Chi, S. Zheng, and X. Zhang, "High-sensitivity temperature sensor based on an optoelectronic oscillator," *Appl. Opt.*, vol. 53, no. 22, pp. 5084–5087, Aug. 2014.

[86] O. Okusaga *et al.*, "The OEO as an acoustic sensor," in *Proc. Joint Eur. Freq. Time Forum Int. Freq. Control Symp.*, Prague, Czech Republic, Jul. 2013, pp. 66–68.

[87] C. H. Lee and S. H. Yim, "Optoelectronic oscillator for a measurement of acoustic velocity in acousto-optic device," *Opt. Exp.*, vol. 22, no. 11, pp. 13634–13640, May 2014.

[88] X. S. Yao and G. Lutes, "A high-speed photonic clock and carrier recovery device," *IEEE Photon. Technol. Lett.*, vol. 8, no. 5, pp. 688–691, May 1996.

[89] F. Cisternino, R. Girardi, S. Römisch, R. Calvani, E. Riccardi, and P. Garino, "A novel approach to pre-scaled clock recovery in OTDM systems," in *Proc. Eur. Conf. Opt. Commun.*, Madrid, Spain, Sep. 1998, pp. 477–478.

[90] C. Y. Lou, L. Huo, G. Q. Chang, and Y. Z. Gao, "Experimental study of clock division using the optoelectronic oscillator," *IEEE Photon. Technol. Lett.*, vol. 14, no. 8, pp. 1178–1180, Aug. 2002.

[91] J. Lasri, P. Devgan, R. Tang, and P. Kumar, "Ultralow timing jitter 40-Gb/s clock recovery using a self-starting optoelectronic oscillator," *IEEE Photon. Technol. Lett.*, vol. 16, no. 1, pp. 263–265, Jan. 2004.

[92] H. Tsuchida and M. Suzuki, "40-Gb/s optical clock recovery using an injection-locked optoelectronic oscillator," *IEEE Photon. Technol. Lett.*, vol. 17, no. 1, pp. 211–213, Jan. 2005.

[93] H. Tsuchida, "Subharmonic optoelectronic oscillator," *IEEE Photon. Technol. Lett.*, vol. 20, no. 17, pp. 1509–1511, Sep. 1, 2008.

[94] S. Pan and J. Yao, "Optical clock recovery using a polarization-modulator-based frequency-doubling optoelectronic oscillator," *J. Lightw. Technol.*, vol. 27, no. 16, pp. 3531–3539, Aug. 15, 2009.

[95] H. Tsuchida, "Simultaneous prescaled clock recovery and serial-to-parallel conversion of data signals using a polarization modulator-based optoelectronic oscillator," *J. Lightw. Technol.*, vol. 27, no. 17, pp. 3777–3782, Sep. 1, 2009.

[96] Q. Wang *et al.*, "Gaussian-like dual-wavelength prescaled clock recovery with simultaneous frequency-doubled clock recovery using an optoelectronic oscillator," *Opt. Exp.*, vol. 22, no. 3, pp. 2798–2806, Feb. 2014.

[97] Y. Xing, L. Huo, Q. Wang, X. Jiang, H. Li, and C. Lou, "Time-lens based optoelectronic oscillator for simultaneous clock recovery and demultiplexing of OTDM signal," in *Proc. 39th Eur. Conf. Opt. Commun.*, London, U.K., Sep. 2013, pp. 1–3.

[98] V. J. Urick, P. S. Devgan, J. D. McKinney, F. Bucholtz, and K. J. Williams, "Channelisation of radio-frequency signals using opto-electronic oscillator," *Electron. Lett.*, vol. 45, no. 24, pp. 1243–1244, Nov. 2009.

[99] P. S. Devgan, M. W. Pruessner, V. J. Urick, and K. J. Williams, "Detecting low-power RF signals using a multimode optoelectronic oscillator and integrated optical filter," *IEEE Photon. Technol. Lett.*, vol. 22, no. 3, pp. 152–154, Feb. 1, 2010.

[100] P. S. Devgan, V. J. Urick, and K. J. Williams, "Detection of low-power RF Signals using a two laser multimode optoelectronic oscillator," *IEEE Photon. Technol. Lett.*, vol. 24, no. 10, pp. 857–859, May 15, 2012.

[101] P. S. Devgan, V. J. Urick, and K. J. Williams, "Multi-mode optoelectronic oscillator," U.S. Patent 8 824 901 B2, Sep. 2, 2014.

[102] I. Ozdur, D. Mandridis, M. U. Piracha, M. Akbulut, N. Hoghooghi, and P. J. Delfyett, "Optical frequency stability measurement using an etalon-based optoelectronic oscillator," *IEEE Photon. Technol. Lett.*, vol. 23, no. 4, pp. 263–265, Feb. 15, 2011.

[103] H. Chen, M. Xia, M. Sun, X. Sun, C. Cai, and X. Sun, "A distributed online optical power monitor based on optoelectronic oscillator," *Proc. SPIE*, vol. 9362, p. 936219, Mar. 2015.

[104] D. Lu, J. Chen, X. Zhao, L. Huo, and C. Lou, "Fractional frequency multiplication by using optically injection locked optoelectronics oscillator," in *Proc. Conf. Lasers Electro-Opt.*, Baltimore, MD, USA, May 2011, pp. 1–2.

[105] Y. Jiang *et al.*, "Frequency locked single-mode optoelectronic oscillator by using low frequency RF signal injection," *IEEE Photon. Technol. Lett.*, vol. 25, no. 4, pp. 382–384, Feb. 15, 2013.

[106] O. Okusaga *et al.*, "Spurious mode reduction in dual injection-locked optoelectronic oscillators," *Opt. Exp.*, vol. 19, no. 7, pp. 5839–5854, Mar. 2011.

[107] X. S. Yao, L. Davis, and L. Maleki, "Coupled optoelectronic oscillators for generating both RF signal and optical pulses," *J. Lightw. Technol.*, vol. 18, no. 1, pp. 73–78, Jan. 2000.

[108] G. Chang, C. Leu, Y. Gao, and B. Zhou, "A self-pulse-injection locked optoelectronic oscillator used as clock extractor," in *Proc. Conf. Lasers Electro-Opt.*, San Francisco, CA, USA, May 2000, pp. 326–327.

[109] S. Ozharar, I. Ozdur, F. Quinlan, P. J. Delfyett, J. J. Plant, and P. W. Juodawlkis, "Ultra stable coupled optoelectronic oscillator based on slab-coupled optical waveguide amplifier," in *Proc. Conf. Lasers Electro-Opt.*, San Jose, CA, USA, May 2008, pp. 1–2.

[110] F. Quinlan, C. Williams, S. Ozharar, S. Gee, and P. J. Delfyett, "Self-stabilization of the optical frequencies and the pulse repetition rate in a coupled optoelectronic oscillator," *J. Lightw. Technol.*, vol. 26, no. 15, pp. 2571–2577, Aug. 1, 2008.

[111] W. Loh *et al.*, "Low-noise RF-amplifier-free slab-coupled optical waveguide coupled optoelectronic oscillators: Physics and operation," *Opt. Exp.*, vol. 20, no. 17, pp. 19420–19430, Aug. 2012.

[112] C. Williams, J. D. Rodriguez, D. Mandridis, and P. J. Delfyett, "Noise characterization of an injection-locked COEO with long-term stabilization," *J. Lightw. Technol.*, vol. 29, no. 19, pp. 2906–2912, Oct. 1, 2011.

[113] W. Li, F. Kong, and J. Yao, "Stable and frequency-hopping-free microwave generation based on a mutually injection-locked opto-electronic oscillator and a dual-wavelength single-longitudinal-mode fiber laser," *J. Lightw. Technol.*, vol. 32, no. 21, pp. 3572–3577, Nov. 1, 2014.

[114] D. Eliyahu, K. Sariri, M. Kamran, and M. Tokhmakhian, "Improving short and long term frequency stability of the opto-electronic oscillator," in *Proc. IEEE Int. Freq. Control Symp. PDA Exhibit.*, New Orleans, LA, USA, May 2002, pp. 580–583.

[115] D. T. Spencer, S. Srinivasan, A. Bluestone, D. Guerra, L. Theogarajan, and J. E. Bowers, "A low phase noise dual loop optoelectronic oscillator as a voltage controlled oscillator with phase locked loop," in *Proc. IEEE Photon. Conf.*, San Diego, CA, USA, Oct. 2014, pp. 412–413.

[116] S. Jia *et al.*, "A novel highly stable dual-wavelength short optical pulse source based on a dual-loop optoelectronic oscillator with two wavelengths," *IEEE Photon. J.*, vol. 7, no. 4, Aug. 2015, Art. ID 1502611.

[117] Y. Zhang, D. Hou, and J. Zhao, "Long-term frequency stabilization of an optoelectronic oscillator using phase-locked loop," *J. Lightw. Technol.*, vol. 32, no. 13, pp. 2408–2414, Jul. 1, 2014.

[118] E. D. Black, "An introduction to Pound–Drever–Hall laser frequency stabilization," *Amer. J. Phys.*, vol. 69, no. 1, pp. 79–87, Jan. 2001.

[119] K. Saleh, G. Lin, and Y. K. Chembo, "Effect of laser coupling and active stabilization on the phase noise performance of optoelectronic microwave oscillators based on whispering-gallery-mode resonators," *IEEE Photon. J.*, vol. 7, no. 1, Dec. 2014, Art. ID 5500111.

[120] M. Bagnell, J. Davila-Rodriguez, and P. J. Delfyett, "Millimeter-wave generation in an optoelectronic oscillator using an ultrahigh finesse etalon as a photonic filter," *J. Lightw. Technol.*, vol. 32, no. 6, pp. 1063–1067, Mar. 15, 2013.

[121] P. Salzenstein, V. B. Voloshinov, and A. S. Trushin, "Investigation in acousto-optic laser stabilization for crystal resonator-based optoelectronic oscillators," *Opt. Eng.*, vol. 52, no. 2, p. 024603, Feb. 2013.

[122] S. Romisch and A. De Marchi, "Noise predictions for optoelectronic oscillators using different models," in *Proc. Int. Freq. Control Symp.*, Besancon, France, Apr. 1999, pp. 1100–1104.

[123] S. Romisch, J. Kitching, E. Ferre-Pikal, L. Hollberg, and F. L. Walls, "Performance evaluation of an optoelectronic oscillator," *IEEE Trans. Ultrason., Ferroelectr., Freq. Control*, vol. 47, no. 5, pp. 1159–1165, Sep. 2000.

[124] Y. K. Chembo, K. Volyanskiy, L. Larger, E. Rubiola, and P. Colet, "Determination of phase noise spectra in optoelectronic microwave oscillators: A Langevin approach," *IEEE J. Quantum Electron.*, vol. 45, no. 2, pp. 178–186, Feb. 2009.

[125] D. Lee, H. Yoon, P. Kim, J. Park, and N. Park, "Optimization of SNR improvement in the noncoherent OTDR based on simplex codes," *J. Lightw. Technol.*, vol. 24, no. 1, pp. 322–328, Jan. 2006.

[126] Z. N. Wang *et al.*, "Phase-sensitive optical time-domain reflectometry with Brillouin amplification," *Opt. Lett.*, vol. 39, no. 15, pp. 4313–4316, Aug. 2014.

[127] X. Fan, Y. Koshikiya, and F. Ito, "Phase-noise-compensated optical frequency domain reflectometry with measurement range beyond laser coherence length realized using concatenative reference method," *Opt. Lett.*, vol. 33, no. 22, pp. 3227–3229, Nov. 2007.

[128] X. Fan, Y. Koshikiya, and F. Ito, "Noise of long-range optical frequency domain reflectometry after optical source phase noise compensation," *Proc. SPIE*, vol. 7503, p. 75032E, Oct. 2009.

[129] *Micro-Opto-Electronic Oscillator (uOEO)*, [Online]. Available: http://www.oewaves.com/products/item/85-micro-opto, accessed September 15, 2015.
[130] K. Volyanskiy, P. Salzenstein, H. Tavernier, M. Pogurmirskiy, Y. K. Chembo, and L. Larger, "Compact optoelectronic microwave oscillators using ultra-high Q whispering gallery mode disk-resonators and phase modulation," *Opt. Exp.*, vol. 18, no. 21, pp. 22358–22363, Oct. 2010.
[131] J. Li, H. Lee, and K. J. Vahala, "Microwave synthesizer using an on-chip Brillouin oscillator," *Nature Commun.*, vol. 4, no. 12, p. 2097, Jun. 2013.
[132] W. Liang *et al.*, "High spectral purity Kerr frequency comb radio frequency photonic oscillator," *Nature Commun.*, vol. 6, p. 7957, Aug. 2015.
[133] M. R. Foreman, J. D. Swaim, and F. Vollmer, "Whispering gallery mode sensors," *Adv. Opt. Photon.*, vol. 7, no. 2, pp. 168–240, Jun. 2015.
[134] R. Soref, "The past, present, and future of silicon photonics," *IEEE J. Sel. Topics Quantum Electron.*, vol. 12, no. 6, pp. 1678–1687, Nov./Dec. 2006.
[135] B. Jalali and S. Fathpour, "Silicon photonics," *J. Lightw. Technol.*, vol. 24, no. 12, pp. 4600–4615, Dec. 2006.
[136] J. Leuthold, C. Koos, and W. Freude, "Nonlinear silicon photonics," *Nature Photon.*, vol. 4, pp. 535–544, Jul. 2010.
[137] L. A. Coldren *et al.*, "High performance InP-based photonic ICs—A tutorial," *J. Lightw. Technol.*, vol. 29, no. 4, pp. 554–570, Feb. 15, 2011.
[138] M. J. R. Heck *et al.*, "Hybrid silicon photonic integrated circuit technology," *IEEE J. Sel. Topics Quantum. Electron.*, vol. 19, no. 4, Jul./Aug. 2012, Art. ID 6100117.
[139] D. Marpaung, C. Roeloffzen, R. Heideman, A. Leinse, S. Sales, and J. Capmany, "Integrated microwave photonics," *Lasers Photon. Rev.*, vol. 7, no. 4, pp. 506–538, Jul. 2013.
[140] C. G. H. Roeloffzen *et al.*, "Silicon nitride microwave photonic circuits," *Opt. Exp.*, vol. 21, no. 19, pp. 22937–22961, Jun. 2013.
[141] J. Wu *et al.*, "Non-blocking 2×2 switching unit based on nested silicon microring resonators with high extinction ratios and low crosstalks," *Chin. Sci. Bull.*, vol. 59, no. 22, pp. 2702–2708, Aug. 2014.
[142] L. Zhou, J. Xie, and J. Chen, "All-optical wavelength converter using a microdisk resonator integrated with *p-n* junctions," *Chin. Sci. Bull.*, vol. 59, no. 22, pp. 2709–2716, Aug. 2014.
[143] N. Dupuis *et al.*, "30-Gb/s optical link combining heterogeneously integrated III–V/Si photonics with 32-nm CMOS circuits," *J. Lightw. Technol.*, vol. 33, no. 3, pp. 657–662, Feb. 1, 2015.
[144] Z. Cao *et al.*, "Integrated remotely tunable optical delay line for millimeter-wave beam steering fabricated in an InP generic foundry," *Opt. Lett.*, vol. 40, no. 17, pp. 3930–3933, Sep. 2015.
[145] S. Iezekiel, M. Burla, J. Klamkin, D. Marpaung, and J. Capmany, "RF engineering meets optoelectronics: Progress in integrated microwave photonics," *IEEE Microw. Mag.*, vol. 16, no. 8, pp. 28–45, Sep. 2015.

**Xihua Zou** (M'10) received the Ph.D. degree from Southwest Jiaotong University, China, in 2009.

He joined the Center for Information Photonics and Communications, Southwest Jiaotong University, in 2009, where he is currently a Full Professor. Since 2014, he has been a Humboldt Research Fellow with the Institute of Optoelectronics, University of Duisburg–Essen, Germany. He once was a Visiting Researcher and a joint training Ph.D. Student of the Microwave Photonics Research Laboratory with the School of Electrical Engineering and Computer Science, University of Ottawa, Ottawa, Canada, in 2011 and in 2007 and 2008, respectively. He was also a Visiting Researcher with the Institut National de la Recherche Scientifique–Énergie, Matériaux et Télécommunications, Montreal, Canada, in 2012. He has authored or coauthored over 70 academic papers in refereed journals. His current interests include microwave photonics, optoelectronic oscillator, radio over fiber, optical pulse generation and compression, fiber Bragg gratings, and optical communications.

Dr. Zou is a member of OSA and SPIE. He was a recipient of the Alexander von Humboldt Research Fellowship (2014), National Outstanding Expert in Science and Technology of China (2014), the Nomination Award for the National Excellent Doctoral Dissertation of China (2011), the Science and Technology Award for Young Scientist of Sichuan Province, China (2013), and the Outstanding Reviewer of Optics Communications (2015). He served as the leading Guest Editor of Special Section on Microwave Photonics in Optical Engineering, SPIE.

**Xinkai Liu** received the B.S. degree in communication engineering from Southwest Jiaotong University, China, in 2008.

He is currently pursuing the Ph.D. degree with the School of Information Science and Technology, Southwest Jiaotong University, China. His research interests include optoelectronic oscillator and microwave photonics.

**Wangzhe Li** received the B.E. degree in electronic science and technology from Xi'an Jiaotong University, Xi'an, China, in 2004, the M.Sc. degree in optoelectronics and electronic science from Tsinghua University, Beijing, China, in 2007, and the Ph.D. degree in electrical engineering from the University of Ottawa, Canada, in 2013. He is currently a Post-Doctoral Researcher with the Department of Electrical and Computer Engineering and Department of Materials, University of California, Santa Barbara, USA. His current research interests include photonic generation of microwave and terahertz signals, arbitrary waveform generation, optoelectronic oscillation, and silicon photonics.

Dr. Li was a recipient of a 2011 IEEE Microwave Theory and Techniques Society Graduate Fellowship and the 2011 IEEE Photonics Society Graduate Fellowship.

**Peixuan Li** received the B.S. degree from Southwest Jiatotong University, Chengdu, China, in 2012, where he is currently pursuing the Ph.D. degree with the School of Information Science and Technology.

His current research interests include microwave photonic processing and generation and fiber communication systems.

**Wei Pan** received the Ph.D. degree from Southwest Jiaotong University, China, in 1999. He is currently a Full Professor and the Dean of the School of Information Science and Technology, Southwest Jiaotong University. His research interests include semiconductor lasers, nonlinear dynamic systems, and optical communications. He has authored over 100 research papers.

Prof. Pan is a member of the Optical Society of America and the Chinese Optical Society.

**Lianshan Yan** received the B.E. degree from Zhejiang University, Hangzhou, China, and the Ph.D. degree from the University of Southern California, Los Angeles. He is currently a Full Professor with Southwest Jiaotong University, Chengdu, China.

Prof. Yan is a Senior Member of the IEEE Photonics Society.

**Liyang Shao** received the Ph.D. degree from Zhejiang University, China, in 2008. From 2006 to 2009, he was with The Hong Kong Polytechnic University, and afterwards worked as a Post-Doctoral Fellow with the Department of Electronics, Carleton University, Canada. He is currently a Full Professor with the School of Information Science and Technology, Southwest Jiaotong University, China. His current research interests are fiber gratings, fiber lasers and sensors, surface plasmon biosensors, and industrial fiber optic sensing system.